University of New Mexico
UNM Digital Repository

Electrical and Computer Engineering ETDs | Engineering ETDs

2-14-2014

REALIZATION OF TEMPERATURE COMPENSATED ALUMINUM NITRIDE MICRORESONATOR FILTERS WITH BANDWIDTHS BEYOND kt2 LIMIT

Janet Nguyen

Follow this and additional works at: https://digitalrepository.unm.edu/ece_etds

Recommended Citation
Nguyen, Janet. "REALIZATION OF TEMPERATURE COMPENSATED ALUMINUM NITRIDE MICRORESONATOR FILTERS WITH BANDWIDTHS BEYOND kt2 LIMIT." (2014). https://digitalrepository.unm.edu/ece_etds/193

This Thesis is brought to you for free and open access by the Engineering ETDs at UNM Digital Repository. It has been accepted for inclusion in Electrical and Computer Engineering ETDs by an authorized administrator of UNM Digital Repository. For more information, please contact disc@unm.edu.

Janet Nguyen
Candidate

Electrical and Computer Engineering
Department

This thesis is approved, and it is acceptable in quality and form for publication:

Approved by the Thesis Committee:

Professor Christos Christodoulou , Chairperson

Professor Mark Gilmore

Dr. Roy Olsson, III

REALIZATION OF TEMPERATURE COMPENSATED ALUMINUM NITRIDE MICRORESONATOR FILTERS WITH BANDWIDTHS BEYOND k_t^2 LIMIT

by

JANET NGUYEN

BACHELOR OF SCIENCE ELECTRICAL ENGINEERING
UNIVERSITY OF NEW MEXICO

THESIS

Submitted in Partial Fulfillment of the
Requirements for the Degree of

Master of Science
Electrical Engineering

The University of New Mexico
Albuquerque, New Mexico

December 2013

DEDICATION

Troy Olsson, the opportunity to be a part of your research team has been the best thing that's ever happened to me. You are in incredible leader and an amazing principle investigator. You have become more than a mentor and advisor; you're my friend and someone who teaches me every day with your example. I've had so much fun while supporting your challenging visions, and I'm grateful to you for the opportunity and inspiration from your work to get this graduate degree.

David Henry, thank you for your honesty and support. You stepped in to protect me when I was being disregarded, even when you did not agree with me. You've given me opportunities to grow so that I might become a good engineer. You took your own time to show up and be a supportive and comforting presence when I was terrified. Thank you for being a wonderful friend and letting me observe your talent as a scientist and leader so that I can emulate your example as I progress.

Travis Young, I respect you so much and I treasure your friendship. You are an incredible human being and I thank you for the support you've generously offered. You never faulted me for my quirks and you heard me when no one else did. You remind me to laugh when I'm struggling. Your strength of character in how you approach life inspires me.

Bongsang Kim, more than anyone else, you taught me what it means to be a great engineer. You are brilliant, funny, and strong-willed. I was so lucky to have had you as an office-mate and you became like a brother to me. I enjoyed working for you and learning from you. Thank you for your patience and your exceptional example. You are the caliber of engineer I strive to be able to become.

ACKNOWLEDGEMENTS

Thank you, Dr. Troy Olsson, for having given me the opportunity to learn and contribute to RF MEMS through support of your work. I sought long and hard for an electrical engineering field that fascinated and intrigued me. Your research has given me exposure to technology and developments that I never could have imagined I'd be able to witness. Thank you for teaching me, challenging me, and helping me grow from my mistakes.

Sincere thanks, also, to Dr. Chris Nordquist who has been my "RF Professor". Chris, I've relied heavily on your expertise, brilliance, and patience to ensure the integrity of our work. Thank you for being someone I count on whenever I have any questions or confusion. Thank you for being someone who works so hard and helps so many people to make sure important work progresses.

REALIZATION OF TEMPERATURE COMPENSATED ALUMINUM NITRIDE MICRORESONATOR FILTERS WITH BANDWIDTHS BEYOND k_t^2 LIMIT

By Janet Nguyen

B.S., Electrical Engineering, University of New Mexico, Albuquerque 2008
M.S., Electrical Engineering, University of New Mexico, Albuquerque 2013

ABSTRACT

There is currently a gap in the technologies available for realizing miniature, temperature compensated RF filters with fractional bandwidths of ~1%. This presentation will cover the development of miniature filters based on temperature compensated aluminum nitride microresonators that have fractional bandwidths exceeding the microresonator coupling coefficient, k_t^2, limit of 0.3%. A method is presented that offers the flexibility of using low Q reactive components to couple temperature compensated aluminum nitride microresonators with bandwidths ranging from extremely narrow (0.05%), as limited by the Q of the resonators, to fairly wide (~1.5%) depending on the coupling network topology. This method overcomes the limiting effect on filter bandwidth due to piezoelectric resonators' k_t^2 material property and makes possible full, on-chip integration of an RF filter's resonators, coupling networks, and matching networks. This coupling method maintains the benefits of series-cascaded resonator filters such as simplicity of design, out of band rejection, and single-ended port architecture. The filter synthesis method is demonstrated in a 3-pole, temperature compensated AlN microresonator filter that achieves a fractional bandwidth of 1.2% at a center frequency of approximately 500 MHz and an insertion loss of 5.4 dB. Based on the measured temperature coefficient of frequency of the resonators that comprise the filter, the center frequency of the filter will drift by 240 kHz from -55 to 125 °C, which is less than 0.05% of the filter 3 dB bandwidth. The narrow bandwidth and excellent temperature stability will lead to RF systems with improved sensitivity and that are more robust to out of band jammers.

Table of Contents

DEDICATION iii
ACKNOWLEDGEMENTS iv
ABSTRACT v
Table of Contents vi
CHAPTER 1 1
Introduction 1
Resonator Figures of Merit 3
Competing Technologies 5
CHAPTER 2 8
AlN Microresonator Fabrication 8
AlN Microesonator Operation 12
AlN Microresonator Equivalent Circuit 13
CHAPTER 3 17
AlN Microresonator Parameters Extraction 17
Filter Design 19
Motional Impedance Optimization 20
Resonator Coupling 23
Matching Network 39
Filter Layout 42
CHAPTER 4 46
Measurements 46
CHAPTER 5 52
Conclusions 52
WORKS CITED 54

Table of Figures

Figure 1: (a) Top-down view of AlN microresonator (b) 3-D view of AlN temperature compensated AlN bar-shaped microresonator 8
Figure 2: AlN Piezoelectric Vibration Modes (a) Width-extensional mode (b) Shear mode (c) Thickness mode 9
Figure 3: Process Flow for temperature compensated AlN microresonators..... 12
Figure 4: Diagram showing piezoelectric transduction of an AlN microresonator13
Figure 5: Cross-sectional diagram and equivalent circuit model for a single temperature compensated AlN microresonator 14
Figure 6: Layout of two 8-finger electrode temperature compensated AlN microresonators in parallel. 16
Figure 7: In both figures: blue=four fingers, black=6 fingers, red=8 fingers, orange=9 fingers. 17
Figure 8: Modeled and measured transmission (S21) and reflection (S11) parameters for a 4-finger electrode AlN temperature compensated microresonator..... 18
Figure 9: Three pole, synchronous filter design with base resonators having (a) R_x too low (b) optimized R_x (c) R_x too high 21
Figure 10: Equivalent circuit for a two-pole, series cascaded AlN microresonator filter without any external coupling components. Because of the intrinsic C_o elements, there is a built-in coupling network that limits the filter bandwidth. 24
Figure 11: Two-resonator, synchronous filter equivalent circuit. AlN Microresonator 1 is exactly identical to AlN Microresonator 2 with the values in the table above. 26
Figure 12: Two-pole, synchronous filter with external shunt inductor coupling. .. 26
Figure 13: (a) Admittance magnitude and phase of just the coupling network of Figure 12 with Lshunt=10 nH, C_{o1}=C_{o2}=5.062 pF. (b) S-parameters of the entire filter circuit of Figure 12 with Lshunt=10 nH (green and purple), and the filter circuit of Figure 10 without Lshunt (blue and red), and the values in Table 1: Equivalent circuit values for a parallel configuration of 15, 4-finger electrode AlN microresonatorsTable 1. 27
Figure 14: (a) Impedance of just the coupling network of Figure 12 with Lshunt=5 nH, C_{o1}=C_{o2}=5.062 pF (b) S-parameters of the entire filter circuit of Figure 12 with Lshunt=5 nH (green and purple), and the filter circuit of Figure 10 without Lshunt (blue and red), and the values in Table 1: Equivalent circuit values for a parallel configuration of 15, 4-finger electrode AlN microresonatorsTable 1. 29
Figure 15: (a) Impedance of the coupling network when Lshunt=15 nH (b) S-parameters of the entire filter circuit of Figure 12 with Lshunt=15 nH (green and purple), and the filter circuit of Figure 10 without Lshunt (blue and red), and the

values in Table 1: Equivalent circuit values for a parallel configuration of 15, 4-finger electrode AlN microresonatorsTable 1. 30
Figure 16: Effect of coupling network Q on filter transmission parameters. Q of Co1 and Co2 is 35, and Q of Lshunt is 20. 31
Figure 17: Effect of Q on filter poles 32
Figure 18: Two-pole synchronous filter with external inductor pi-network coupling. 33
Figure 19: Two-pole synchronous filter with an external series inductor coupling. 34
Figure 20: (a) Admittance magnitude and phase of only the coupling network of Figure 19 with Lseries=20 nH, C_{o1}=C_{o2}=5.062 pF (b) S-parameters of the entire filter circuit of Figure 19 with Lseries=20 nH (green and purple), and the filter circuit of Figure 10 without Lseries (blue and red), and the values in Table 1: Equivalent circuit values for a parallel configuration of 15, 4-finger electrode AlN microresonatorsTable 1. 35
Figure 21: (a) Admittance magnitude and phase of only the coupling network of Figure 19 with Lseries=40 nH, C_{o1}=C_{o2}=5.062 pF. (b) S-parameters of the entire filter circuit of Figure 19 with Lseries=40 nH (green and purple), and the filter circuit of Figure 10 without Lseries (blue and red), and the values in Table 1: Equivalent circuit values for a parallel configuration of 15, 4-finger electrode AlN microresonatorsTable 1. 36
Figure 22: Filter coupling network with an inductor pi-network schematic. 36
Figure 23: (a) Admittance magnitude and phase of the coupling network of Figure 22 with Lshunt=20 nH, Lseries=1 nH, C_{o1}=C_{o2}=5.062 pF. (b) S-parameters of the entire filter circuit of Figure 18 with Lshunt=20 nH, Lseries=1 nH (green and purple), and the filter circuit of Figure 10 without an external coupling components (blue and red), and the values in Table 1: Equivalent circuit values for a parallel configuration of 15, 4-finger electrode AlN microresonatorsTable 1. 37
Figure 24: S-parameters of the entire filter circuit of Figure 18 with Lshunt=26 nH, Lseries=33 nH (green and purple), and the filter circuit of Figure 10 without an external coupling components (blue and red), and the values in Table 1: Equivalent circuit values for a parallel configuration of 15, 4-finger electrode AlN microresonatorsTable 1. 38
Figure 25: Equivalent circuit for three-pole synchronous filter with external inductor pi-network coupling 39
Figure 26: Transmission and reflection parameters of the entire three pole filter circuit Figure 25 when Lshunt=26nH and Lseries=33nH, overlaid on same parameters for the two-pole filter with no external coupling components. 39

Figure 27: Unmatched 3-pole filter simulated S-parameters in log-magnitude form and on a Smith Chart 40
Figure 28: Impedance matched 3-pole filter simulated S-parameters parameters in log-magnitude form and on a Smith Chart. Bandwidth=5.3MHz at a center frequency of 500.475MHz. 40
Figure 29: (a) Unmatched, 500 MHz filter's simulated group delay (b) Same parameters for the filter once matched to 50Ω termination impedance. 41
Figure 30: Complete 500MHz filter design with 5MHz bandwidth equivalent circuit with coupling networks (red boxes) and matching networks (blue boxes). The crystal resonator components each represent 15 temperature compensated AlN microresonator circuits in parallel. 41
Figure 31: Microscope picture of partially fabricated inductor pi-network to be used for on-chip integration with filter. 42
Figure 32: (a) Layout of one of the three AlN microresonator's needed for the filter. This resonator is made up of 15 identical four-finger electrode individual microresonators connected in parallel. (b) Layout of one of the four-finger electrode AlN microresonators. 43
Figure 33: Close-up of one side of a four-finger electrode temperature compensated AlN microresonator. 43
Figure 34: (a) Layout of the three, temperature compensated AlN microresonators for the filter design (b) Fabricated resonators. 45
Figure 35: S-parameters for three, temperature compensated AlN micreosresonators on a single die. 47
Figure 36: Genesys simulator integrating resonator measurements with coupling networks (red boxes) and matching networks (blue boxes). 47
Figure 37: Simulation data using real resonator measurements with the inductor and capacitor coupling and matching components integrated. 48
Figure 38: S-parameters comparing the measured data with the original filter design downshifted in frequency only. The original designed coupling and matching network components were maintained. 49
Figure 39: Group delay for the filter response using measured data versus the original filter design downshifted in frequency only. The original designed coupling and matching network components were maintained. 49

CHAPTER 1

Introduction

Wireless communication systems often need to operate in environments where there is limited spectrum allocated per user in the presence of strong interferers. These conditions demand receivers that are both highly selective, to be able to receive on very narrow-band channels, and also very sensitive, operating in weak signal conditions. Selective RF filters at high frequencies require difficult to achieve quality factors even with the most current filter technologies (1). This problem is often solved with superheterodyne receivers. These receivers use a local oscillator to convert the front-end RF signals to a lower, fixed, intermediate frequency (IF) signal. Since quality factor (Q) is proportional to center frequency divided by 3dB bandwidth, this lowers the Q requirements for the electronic filters downstream in the receiver's signal processing path. The superheterodyne architecture is robust against interferers since it allows a single user to operate in different channels of the same band by changing the local oscillator frequency. Superheterodyne schemes, due to their higher operating IF, are also able to reject image frequencies, giving them superior selectivity and sensitivity when compared to low-IF receiver designs (2).

As one of the key components in the superheterodyne architecture, IF filters have their own requirements and specifications. These requirements are: frequency stability over operating temperature, insertion loss, 3 dB bandwidth,

isolation between the filter's insertion loss and the stop-band rejection level, and the shape factor. The roll-off rate, or shape factor, is the ratio of bandwidths at different attenuation values that determines the cutoff frequencies. Physical size, absolute group delay, and amplitude and group delay ripple are other common IF filter specifications.

IF filters can be synthesized by the coupling of resonant circuits (3), and utilize passive reactive components at their input and output to perform impedance matching to the circuit that will use them. Resonators are thus the foundational component for IF filters and resonator design and functionality are of the utmost importance in filter performance.

When designing resonators, especially for wireless communications, considerations such as physical size and cost make microelectromechanical system (MEMS) acoustic resonators an attractive technology. Acoustic resonators are miniaturized, micron-scale, resonators that utilize mechanical waves in solids. Wave velocities in solid materials are a factor of ~10,000 slower than the propagation velocity of electromagnetic waves. Since wavelength is proportional to propagation velocity divided by frequency, this scaling of the velocity allows for resonator designs using much smaller wavelengths than their electromagnetic counterparts for given frequencies. Fabrication of MEMS resonators using tools and processes standard to CMOS manufacturing makes the mass production of these resonators an affordable benefit.

A technology that has the parameters needed to create IF filters and fill a gap that currently exists for this type of filter component are aluminum nitride (AlN) microresonators (4). AlN microresonators are acoustic MEMS resonators that are fabricated using standard CMOS processes. As such, they offer the capability of being designed on-chip, fully integrated with the necessary coupling and impedance matching circuit networks to create IF filters. They can also be temperature compensated to minimize frequency shifts due to changes in operating temperature.

Resonator Figures of Merit

As the fundamental component in IF filters, resonator performance determines the specifications achievable by the filter that is comprised of them. The figures of merit (FOM) that characterize resonators, with respect to their use in filter design, are the electromechanical coupling coefficient (k_t^2), quality factor (Q), the $k_t^2 \cdot Q$ product, and the temperature coefficient of frequency.

The coupling coefficient, or k_t^2, of a resonator is a material property, extracted from resonator electrical measurements, that is widely used in the design of RF band-pass filters. Though there is currently no single, accepted definition of resonator coupling coefficient (5), it is a parameter that is used to accurately and directly synthesize band-pass filters with up to 10% relative bandwidths (3). In the case of acoustic resonators, coupling coefficient can be thought of as the efficiency of the conversion between electrical fields and acoustical fields (6).

The coupling coefficient of the resonators that form a filter are the limiting factor in the maximum achievable bandwidth of a filter while maintaining flat pass-bands (7), with higher k_t^2 making wider bandwidth filters possible(6).

The quality factor (Q) of a resonator characterizes the losses in the resonant system and corresponds to the resonator's transmission peak width:

$$Q = 2\pi * \frac{\text{energy stored per cycle}}{\text{energy dissipated per cycle}} = \frac{\text{center frequency}}{\text{3dB bandwidth}}. \qquad [1]$$

Higher quality factor translates to less energy lost in the system which leads to improved filter insertion loss and steeper filter skirts (8). The $k_t^2 \cdot Q$ product is a measure of the resonator's isolation, or the amplitude difference between the maximum resonator transmission and the out-of-band, feed-through transmission level.

Finally, resonators, especially acoustic resonators, depending on their materials, have temperature coefficients of frequency. The elastic modulus of the materials that form the resonators can slightly change depending on operating temperature, leading to frequency changes that need to be considered in filter design. Frequency shifts of RF filters due to changes in temperature require wider filter bandwidths to ensure proper operation over the desired frequency ranges. Having wider bandwidths to compensate for a filter's frequency deviation due to temperature reduces the selectivity and sensitivity of RF receivers.

Competing Technologies

Considering these filter specifications and resonator figures of merit, AlN microresonators are an optimal candidate for low-loss, IF filters requiring relative bandwidths of ~1% that need frequency stability over operating temperature fluctuations. Though their coupling coefficient is not as high as it is for other resonator technologies such as bulk acoustic wave (BAW) resonators, AlN microresonators have fabrication advantages over BAW devices. BAW resonators have their frequencies defined by the thickness of the resonator, a limitation that prevents devices with multiple frequencies from being easily, and affordably, fabricated on a single wafer. At IF frequencies, such as those reported in this work, BAW resonators require thin film thicknesses of ~10 µm, which are difficult to realize and leads to very large devices for a 50 Ω termination impedance. AlN microresonators have their frequencies defined lithographically, allowing multiple frequency devices to be fabricated side-by-side on a single chip in a thin (~ 1 µm) AlN layer, irrespective of the filter frequency. This makes possible the fabrication of an AlN microresonator as a local oscillator reference alongside the IF filter for a superheterodyne receiver circuit, reducing the number of discrete components in the receiver. Because AlN microresonators are fabricated using CMOS compatible processes, these resonant circuits could also be integrated with a CMOS oscillator circuit on a single chip with a very small footprint (9).

Other MEMS resonators, such as electrostatically transduced resonators, can have significantly higher Q than AlN microresonators. This comes at the cost of

much higher motional impedance which complicates resonator integration into RF applications requiring a 50Ω or 75Ω impedance matching. While viable for lower frequency applications (<200MHz) where their impedance values are lower, typical capacitive resonators operating in the ultra high frequency band (UHF), 300 to 3000 MHz, have impedances in the hundreds of kOhms (10). This higher impedance is due to the electrostatic forces being much smaller than the piezoelectric forces generated by similarly sized transducers. This higher impedance becomes problematic at the frequencies used by superheterodyne systems where circuit simplification is an important benefit of the architecture. Most significantly, electrostatic microresonators have very low coupling coefficients, much less than 0.1%, and they cannot be used to synthesize filters with useful bandwidths.

These considerations of k_t^2, Q, and naturally, the $k_t^2 \cdot Q$ product of resonators lead to a choice between quartz surface acoustic wave resonators (SAW), and AlN microresonators as the technologies of interest for filters that are ~1% bandwidth. ST-cut quartz is the primary solution for narrow bandwidth temperature compensated IF filters. These resonators are much larger than AlN microresonators and the k_t^2 of ST-cut quartz is only 0.16%, as opposed to a k_t^2 of ~1% for AlN temperature compensated microresonators. SAW filters are a close competitor to AlN microresonators. SAW resonators with different frequencies can be manufactured on a single chip, but, unlike AlN resonators, which are much more mechanically isolated on the semiconductor substrate, SAW resonators require larger footprints to reduce mechanical crosstalk. SAW

resonators made with piezoelectric materials such as Y-cut lithium tantalate, $LiTaO_3$, have higher k_t^2 than AlN microresonators, but they have temperature coefficients of frequency (TCF) on the order of -45ppm/C˚ (11). X-cut $LiTaO_3$ SAW resonators are able to be temperature compensated, so that filters made with these resonators will not shift in frequency with changes in operating temperature. The k_t^2 of these resonators is significantly lower (0.75%) than the k_t^2 of temperature compensated AlN microresonators (~1%), limiting the maximum filter bandwidth achievable by X-cut $LiTaO_3$ SAWs below that of AlN microresonators. Along with these limitations, these SAW and quartz resonators, because of their orientation dependent, single crystal nature, are difficult to integrate with CMOS technology. Temperature compensated AlN microresonators (12) thus becomes the technology of choice for low-loss, frequency stable, 1% relative bandwidth, IF filters that are difficult to achieve in other technologies.

CHAPTER 2

AlN Microresonator Fabrication

AlN microresonators are piezoelectric, acoustic, MEMS resonators that operate in a lateral, width-extensional mode, Figure 2(a). The resonators work by using the piezoelectric properties of AlN to convert electromagnetic energy from the input port into mechanical (acoustic) vibrations and then back into electromagnetic waves at the output. They are fabricated from thin films stacks into structures that are suspended on high-resistivity silicon substrates.

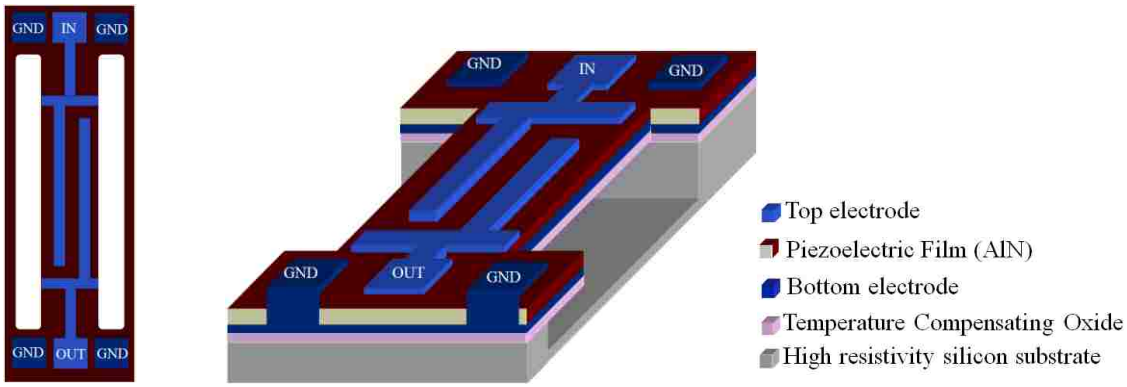

(a) **(b)**

Figure 1: (a) Top-down view of AlN microresonator (b) 3-D view of AlN temperature compensated AlN bar-shaped microresonator

AlN is a piezoelectric material that can be transduced into thickness mode vibrations, shear mode vibrations, and contour mode vibrations; each with its own piezoelectric coefficient (7). Shear modes are difficult to excite in AlN because of how the electrodes must be placed in contact with the piezoelectric

material and thickness modes are used in AlN BAW resonators, where film thickness determines the resonator frequency.

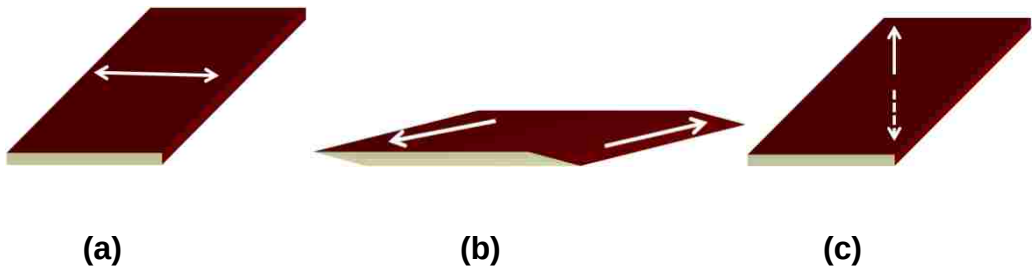

Figure 2: AlN Piezoelectric Vibration Modes (a) Width-extensional mode (b) Shear mode (c) Thickness mode

Because AlN microresonators convert electrical energy into mechanical motion and vice versa, suspension of the resonant structure minimizes acoustic energy loss via mechanical coupling other than through air and the anchor points on either end of the resonator.

Temperature compensated AlN microresonators are fabricated using six photolithographic masks in the CMOS compatible process flow of Figure 3. A brief overview of the fabrication process for these microresonators will be discussed while greater details of the fabrication process can be found in (13) (14). From the bottom up, a high-resistivity silicon wafer, used to minimize parasitic electrical pathways in the semiconductor substrate, has silicon dioxide and then a sacrificial poly-silicon 'release' layer deposited and patterned onto it. Next, a temperature compensating silicon dioxide layer, the thickness of which is designed to passively counteract the negative temperature coefficient (TC) of Young's modulus for AlN is deposited. Silicon dioxide's positive TC of 25ppm/C˚

mechanically compensates the negative TC for AlN microresonators. This reduces the temperature coefficient of frequency of AlN microresonators from from ~ -30ppm/C˚ when uncompensated to 2.5ppm/C˚ (12). The frequency of an AlN resonator is dependent upon the velocity of the acoustic waves within the resonator from Equation [2]. If the effective Young's modulus ($E_{effective}$) of the composite thin film stack that forms the resonator changes, this will change the acoustic wave velocity and thus the frequency of the resonator. For a fixed film thickness, the acoustic velocity stays constant and the frequency of a resonator can be changed by designing the width dimension of a resonator to control the wavelength of the acoustic wave being stored in the resonator. The acoustic propagation velocity is also dependent on the effective density of the resonator, but that does not change appreciably within relevant temperatures (-55 to 125C). The temperature dependent equations that govern frequency design for AlN microresonator are (12):

Variable	Definition	Variable	Definition
f	frequency	t	film thickness
v	acoustic velocity	λ	wavelength
E	Young's modulus	ρ	density
T	temperature		

$$f(T) = \frac{v(T)}{\lambda} \qquad [2]$$

$$v(T) = \sqrt{\frac{E_{effective}(T)}{\rho_{effective}}} \qquad [3]$$

$$E_{effective}(T) = \frac{E_{AlN}(T)*t_{AlN}+E_{SiO2}(T)*t_{SiO2}+E_{Al(T)}*t_{Al}}{t_{AlN}+t_{SiO2}+t_{Al}} \quad [4]$$

To continue with the fabrication procedure, the oxide surrounding the patterned polysilicon release areas are etched and tungsten plugs are deposited. These tungsten plugs serve as an etch stop and allow for electrical contact to the bottom electrode. After the tungsten deposition, the wafer undergoes a chemical mechanical polishing (CMP) to planarize the oxide and tungsten. The metals that form the microresonator bottom electrodes are then sputter deposited and patterned. Then the highly oriented AlN is sputter deposited across the entire wafer. The quality of thin films and bulk single crystals are characterized by a metric known as rocking curves. Rocking curves use Bragg reflections and measure diffracted intensity as a sample is rotated or “rocked” to give a measure of defect density and grain size of crystal lattices (15). These microresonators have 750nm of high quality, Rocking Curve FWHM < 1 degree (16) AlN to give the best possible k_t^2. The AlN is then patterned over the tungsten plugs and the top electrode metals are sputter deposited and patterned. Anisotropic, or vertical, etches are then performed to etch through AlN and the temperature compensating silicon oxide to the sacrificial polysilicon release layer. This etch defines the resonator’s width dimension. Finally, with the polysilicon layer exposed at the top surface, the wafer is placed into a chamber where xenon diflouride, XeF_2, isotropically etches the polysilicon to ‘undercut’ the resonators, leaving a ‘released’, suspended thin-film membrane resonator structure.

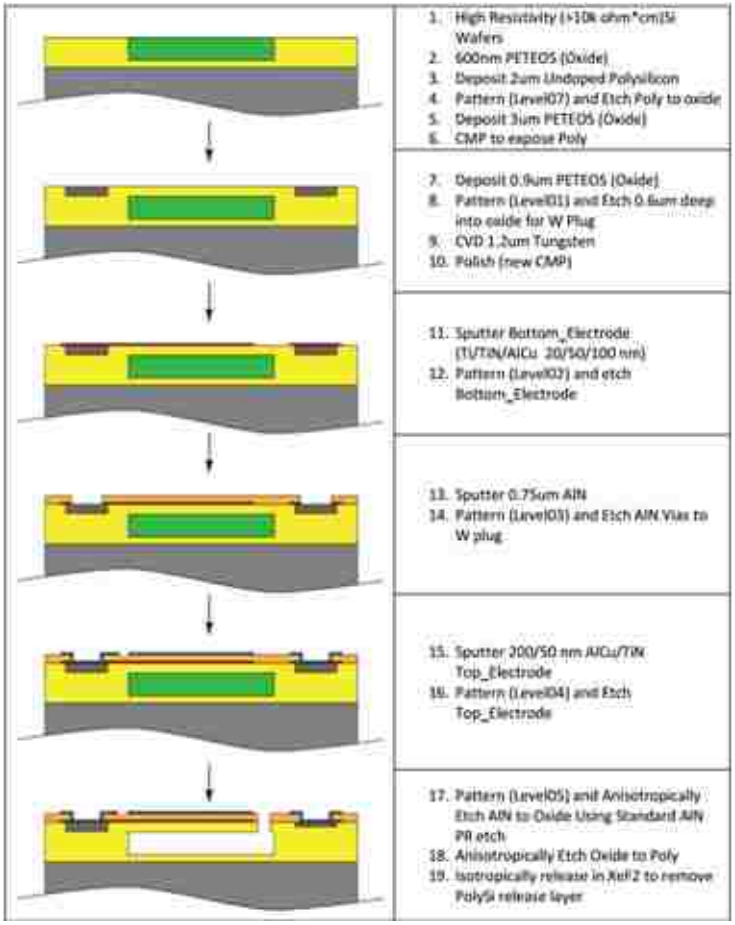

Figure 3: Process Flow for temperature compensated AlN microresonators

AlN Microesonator Operation

AlN microresonators operate by applying electromagnetic fields via an AC voltage between the input electrodes on top of the resonator and the ground plate under the AlN layer. This electromagnetic field induces a strain in the piezoelectric AlN that launches a mechanical, acoustic, standing wave in the resonator's composite thin-film stack. This mechanical wave creates a strain profile that is 90˚ out of phase with the mechanical displacement, and this strain generates a current that is captured by the output electrodes as shown in Figure

4. The frequency of the resonator is defined by the width dimension which has to be an integer multiple of $\frac{\lambda}{2}$ since the transduced standing wave of the resonator is along this dimension. The input and output electrodes are placed at $\frac{\lambda}{2}$ distance apart to maximally transduce a standing wave in the resonator. They are not placed at the very edges of the resonator, at the locations of maximum displacement, because at those locations, there is zero strain and therefore, no current. The width of the electrodes is designed to optimally capture the current at the locations where there is maximum strain while considering the trade-off of increasing the parasitic C_o with wider electrodes, which would reduce k_t^2.

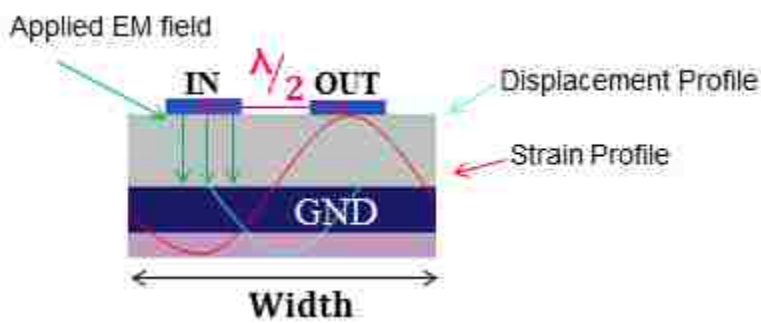

Figure 4: Diagram showing piezoelectric transduction of an AlN microresonator

AlN Microresonator Equivalent Circuit

MEMS acoustic resonators can be modeled as RLC equivalent circuits near their primary resonance (17). Filter synthesis using MEMS resonators has added complexity in that MEMS resonators have their characteristic inductances, capacitances, and motional impedances inter-related by the k_t^2 and Q parameters of each resonator. Those individual equivalent circuit elements cannot be 'disassembled' or used in isolation. In other words, when designing

AlN microresonators, the circuit parameters are inextricably coupled to each other, and changing one parameter affects the others. Designing AlN microresonators requires the interrelated changes and their effects on the k_t^2 and Q to be accounted for and considered. The cross-sectional diagram and equivalent circuit model for temperature compensated AlN microresonators is shown in Figure 5.

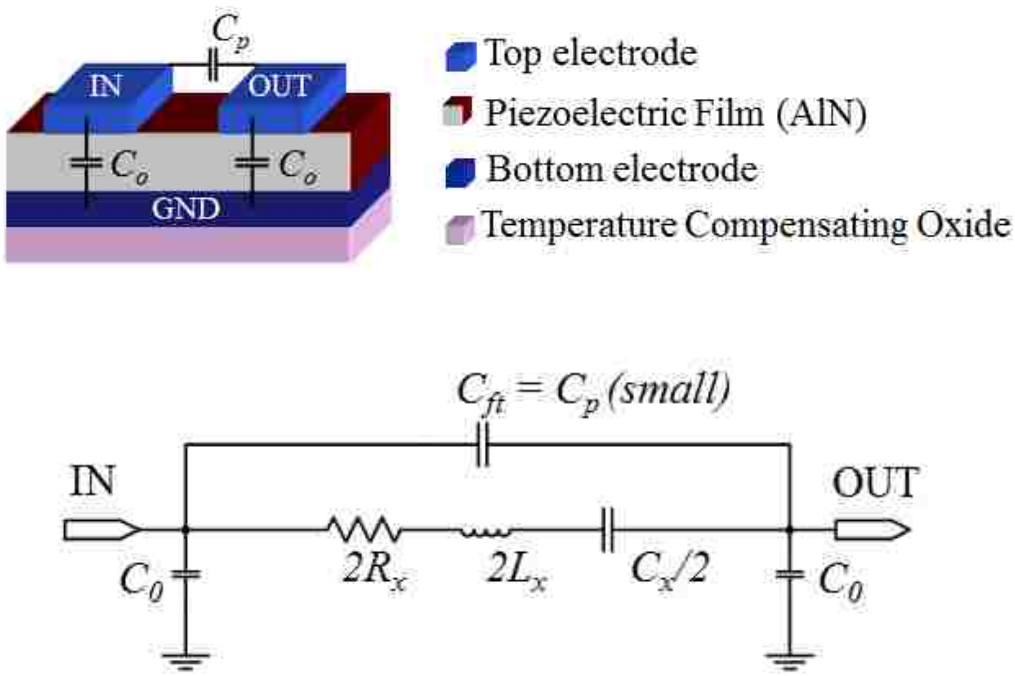

Figure 5: Cross-sectional diagram and equivalent circuit model for a single temperature compensated AlN microresonator

The R_x, C_x, and L_x portion of the equivalent circuit is known as the "motional arm" that is due to mechanical vibrations of the piezoelectric. R_x is known as the motional impedance, which is the circuit loss on resonance. L_x and C_x are the motional inductance and motional capacitance which form the series resonant

circuit that determines the resonant frequency. C_0 is the electrical parasitic shunt capacitance between the electrodes on the top of the resonator and the grounded bottom electrode under the AlN. C_{ft} is the parasitic electrical capacitance between the input and output electrodes and has been determined empirically for temperature compensated AlN microresonators to be ~5fF (16).

The equations that relate these equivalent circuit parameters to resonator figures of merit are (16):

$$\frac{C_X}{C_o} = \frac{8}{\pi^2} k_t^2 \qquad [5]$$

$$R_X = \frac{\pi t \sqrt{E\rho}}{8LnMEQd_{31}^2} = \frac{1}{\omega Q C_X} = \frac{\pi^2}{8} \frac{1}{\omega Q C_o} \frac{1}{k_t^2} \qquad [6]$$

$$Lx = \frac{QR_X}{\omega} \qquad [7]$$

$$Z(C_o) = \frac{1}{j\omega C_o} \qquad [8]$$

$$\frac{Z(C_o)}{R_x} = \frac{8Qk_t^2}{\pi^2} \qquad [9]$$

$$FOM = Q \cdot k_t^2 \qquad [10]$$

Equations [5]-[8] demonstrate the inter-dependence of all three lumped-element components via the resonator Q and k_t^2 parameters as well as frequency, ω. The parasitic capacitance, $C_{0,}$ as it relates to C_x in equation [5], directly affects the k_t^2 of the resonator and the k_t^2 of a resonator is well known to limit the maximum bandwidth of a filter (18). The d_{31} term is the width-extensional mode

piezoelectric coefficient (7) for AlN, shown in Figure 2(a). L is the length of the resonator electrodes that drive and sense the standing wave in the AlN, Figure 6, and n is the number of resonators that are connected in parallel (n=2 for Figure 6), and M is the number of electrodes in a single resonator (M=8 in Figure 6).

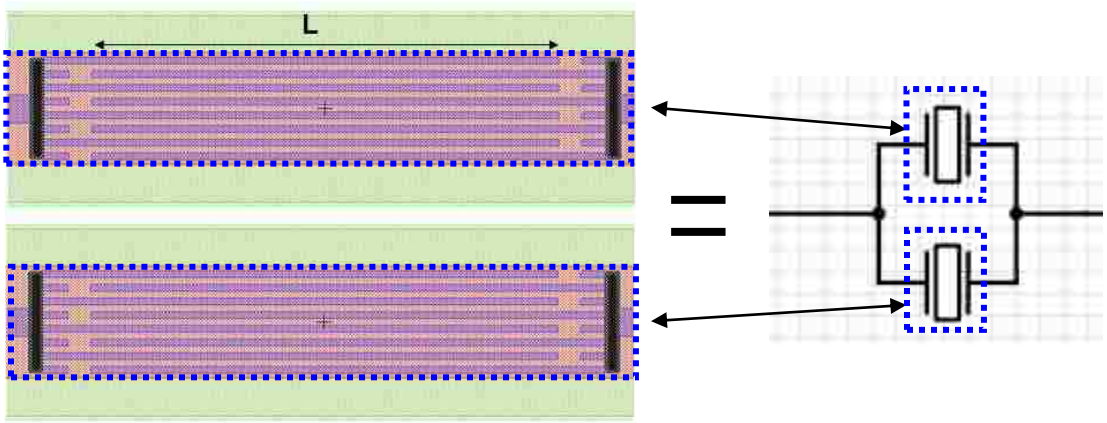

Figure 6: Layout of two 8-finger electrode temperature compensated AlN microresonators in parallel.

CHAPTER 3

AlN Microresonator Parameters Extraction

The first step in designing the filter reported in this work was to select and characterize the resonator which would be used to create the filter. An array of temperature compensated AlN microresonators was designed and fabricated. The temperature compensated AlN microresonators were designed (16) to have different numbers of electrode fingers that would drive different overtone resonant modes. Scattering matrix, or S-parameter, measurements were taken of the temperature compensated AlN microresonators using an Agilent E5071C network analyzer.

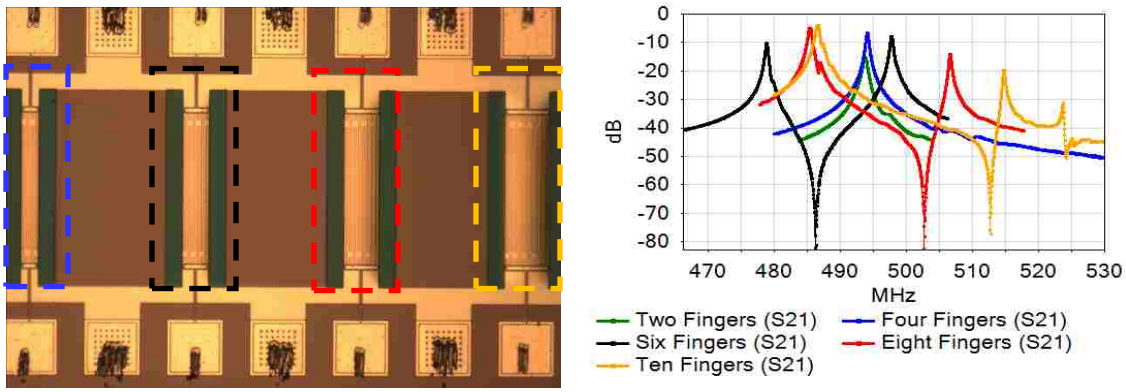

(a) **(b)**

Figure 7: In both figures: blue=four fingers, black=6 fingers, red=8 fingers, orange=9 fingers. (a) Microscope image of four different AlN microresonator designs, each with a different number of fingers. (b) S21 measurements of the temperature compensated AlN microresonators. In 6(b), green=two fingers.

The transmission parameter measurements of Figure 7(b) indicated that the two-finger and four-finger electrode resonator designs had the fewest spurious modes, or modes that are not predicted by the electrical equivalent circuit, which

would severely distort the filter behavior (17). The S-parameter data for the resonators was imported into Genesys RF and Microwave Design Simulation software. Equations [5]-[8] relating the equivalent lumped-element circuit components of the microresonator were entered into the simulator to model the temperature compensated AlN microresonators. The modeled response was then fit to the measured S-parameter data to extract the k_t^2, Q, and R_x values of the resonators. The k_t^2 of all the resonators were identical, but the four-finger electrode design was found to have had the highest Q along with the fewest spurious modes, and was thus selected as the base resonator for this filter design.

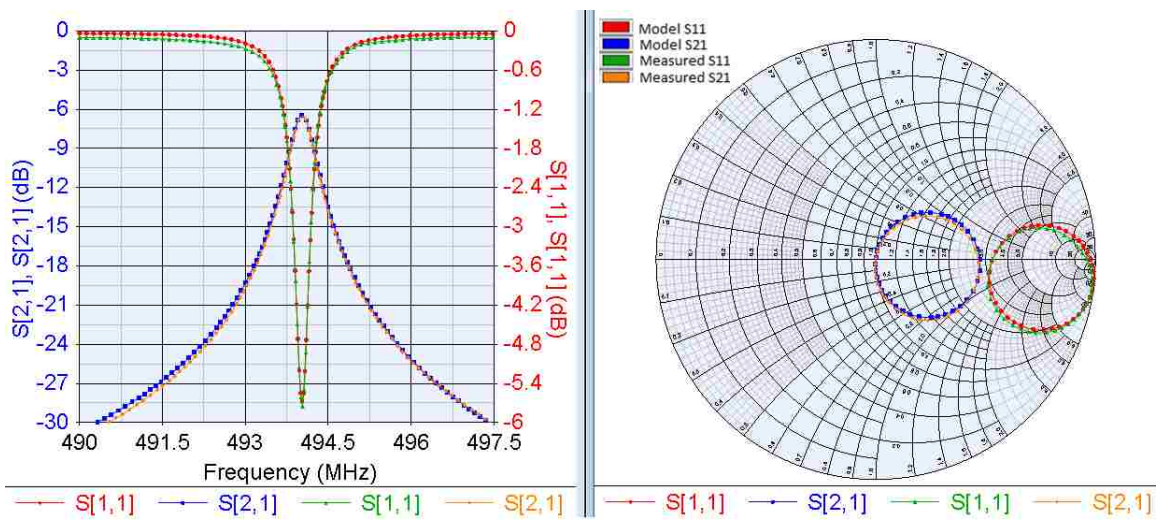

Figure 8: Modeled and measured transmission (S21) and reflection (S11) parameters for a 4-finger electrode AlN temperature compensated microresonator.

Figure 8 shows the measured four-finger electrode resonator's S-parameter measurement and the fitted model in both log-magnitude form and on a Smith Chart. From this analysis, this temperature compensated AlN microresonator

design was found to have k_t^2= 1.00%, Q = 1900, and R_x = 56Ω. From the measured center frequency, and physical dimensions of the resonator, the acoustic velocity of this thin film stack was found to be 7998 m/sec. Because the center frequency of this resonator, 494.03MHz, is very close to the desired center frequency, within 10% (16), of the filter to be designed, this acoustic velocity is a very good estimate of the velocity to be used in the 500MHz filter design since the same thin film stack will be used. Acoustic velocity in thin films varies with the films' thicknesses. If empirical resonator measurements were not available, modeling of the resonator thin film stack is an effective method to calculate the acoustic velocities for different thin film stack thicknesses and for frequencies that are greater than 10% different from the available measurements.

Filter Design

The roll-off, or shape factor, of a filter can be improved by cascading multiple resonators in series. When multiple resonators are cascaded in series, their transmission characteristics are combined and this allows poles, or frequencies of maximum transmission amplitude, to be combined. The combination of multiple resonator stages also improves the filter's selectivity by creating steeper filter skirts to select only the desired pass-band signals and improve stop-band rejection (1).

Band-pass filters using multiple resonators cascaded in series can be designed either synchronously, using resonant sub-circuits that are all at the same center frequency, or asynchronously, with resonant sub-circuits of different frequencies, symmetric about the desired center frequency. Bandwidths of equal size can be realized by either method, but the insertion loss is worse in asynchronous designs, especially for filter circuits with more than two resonant sub-circuits, so synchronously tuned filters are of more practical use (17). To meet the shape-factor and insertion loss requirements for this filter, a synchronous design of three resonator stages was used.

Motional Impedance Optimization

Because of the frequency dependence of R_x, the motional impedance of the resonators used to build the filter need to be optimized. To do that, the three-stage synchronous filter circuit with 50Ω port terminations, with the resonators connected directly in series, is used to characterize the optimal motional impedance needed for the resonators. For too low or too high a motional impedance, the filter response of a three-pole resonator without any external circuit components would become asymmetrical in the pass-band, shown in Figure 9, because the filter would not be properly matched to 50 Ω.

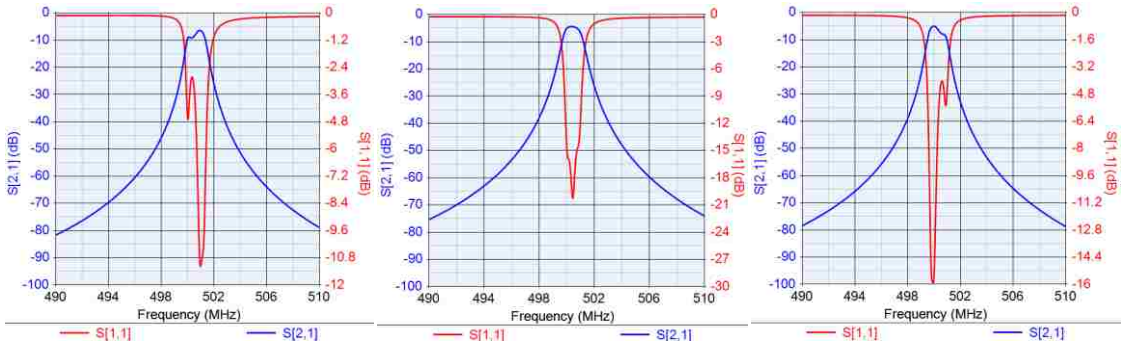

(a) **(b)** **(c)**

Figure 9: Three pole, synchronous filter design with base resonators having (a) R_x too low (b) optimized R_x (c) R_x too high

The optimal motional impedance of the resonators needed for this filter design was 3.7Ω, which is obtained by a parallel circuit combination of fifteen of the individual four-finger electrode temperature compensated AlN microresonators that each had an R_x=56Ω. Analysis of the equivalent circuit for each of the individual resonators, Figure 5, shows that parallel circuit combinations of the same series RLC circuit, results in a resonant circuit with an equivalent R_x that is scaled down by a factor of the number of individual resonators connected in parallel. The other equivalent circuit parameters, C_x, L_x, and C_o are similarly scaled.

The amplitude of a filter's transmission response depends on both dissipative loss and reflection loss. In this filter design, dissipative loss is due primarily to the resonator motional impedance, R_x, and the resistance of any external coupling components, which is related to the Q of the passive reactive components. Though it would have been possible to design this filter to have the same response with a lower R_x, this would have accordingly scaled C_x, L_x, and

C_o. The external impedance matching and coupling components that would be needed in the filter design would also have to be scaled. This motional impedance of 3.7Ω was selected because it resulted in reasonable values of reactive inductances and capacitances for the coupling and impedance matching networks.

Reflection loss occurs when the filter is not impedance matched to the circuit it is connected to. In order to impedance match a filter, one can change the termination impedance that the filter sees at its input and output ports (nominally 50Ω), which effectively changes the "load" that the first and last resonators forming the filter see. When the impedance seen by a resonant circuit is increased, this has the effect of loading the quality factor of the resonator, or widening its 3dB bandwidth. This leads to the parameter known as loaded Q, which accounts for the impedance seen by a resonator, and the unloaded Q, which is the quality factor intrinsic to the resonator. The loaded and unloaded Q can be extracted from an empirical measurement of a resonator by the following equations (16):

$$Q_{loaded} = \frac{R_x}{R_{in}+R_x+R_{out}} * Q_{unloaded} \qquad [12]$$

$$IL = 20\log_{10}\frac{2R_t}{2R_t+R_x} \qquad [13]$$

$$\text{3dB bandwidth} = \frac{\text{center frequency}}{Q_{loaded}} \qquad [14]$$

It is important to note the difference between the use of resonator Q-loading versus Q degradation of a resonator. The relatively high Q of AlN

microresonators makes it possible to create selective filters with steep roll-offs using fewer resonator stages. Loading the Q maintains this out of band rejection benefit of high Q, while simulanteously widening the 3dB bandwidth to smooth out passband ripple. Higher Q resonators are, therefore, desirable, while the option to load the Q can be used to obtain desired pass-band responses. Reflection, or impedance mismatch, losses can be fixed by proper impedance matching, while dissipative losses require higher Q components.

Resonator Coupling

There are several different analytical methods for filter synthesis based on configuring reactive circuits to couple resonators in order to achieve a desired pass-band response. It was predicted in (17) that any reactive components can be used to couple cascaded resonators to form a band-pass filter for standard lumped-element resonator circuit models. The challenge with using these methods on temperature compensated AlN microresonators is that AlN microresonators have the unique characteristic of being relatively high Q (~2000) resonators while having an intrinsically low Q (~35) shunt capacitance element that cannot be treated as an independent discrete lumped-element component. This shunt capacitance, C_o, automatically introduces a lossy, shunt capacitive coupling network, Figure 10, which limits the maximum bandwidth achievable (19) when these resonators are connected in series.

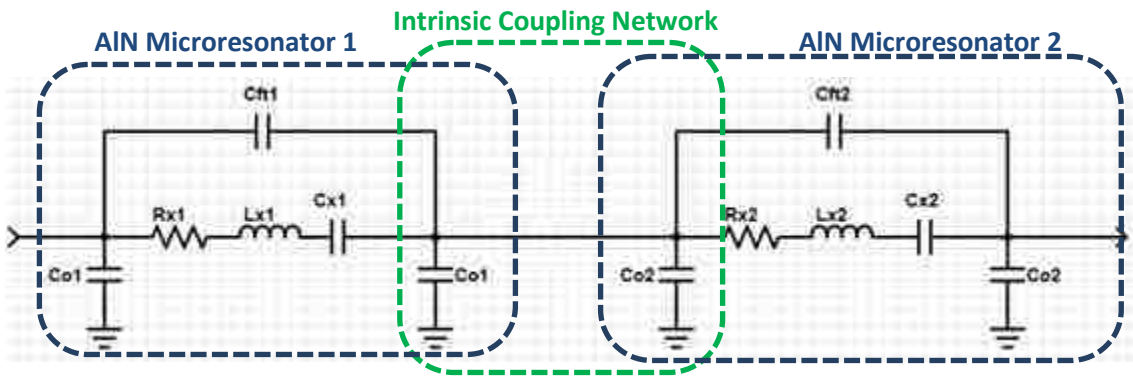

Figure 10: Equivalent circuit for a two-pole, series cascaded AlN microresonator filter without any external coupling components. Because of the intrinsic C_o elements, there is a built-in coupling network that limits the filter bandwidth.

Work done by (19) demonstrates how the poles of a three stage, AlN microresonator filter design, coupled only by the intrinsic C_o of the resonators, has higher order poles that widen the filter bandwidth, depending on the ratio of C_x to C_o. Thus, the ratio of $\frac{C_x}{C_o}$ is known to limit the distance that a resonance is able to be separated from the initial, first-order center frequency of the filter, with wider bandwidths possible for very small C_o. For temperature compensated AlN microresonators, $\frac{C_x}{C_o}$ is ~0.87%, so the pole-splitting effect that widens a filter's bandwidth is already limited because of C_o's relatively high value with respect to C_x. To achieve wider bandwidth filters, C_o needs to be as small as possible. Because of the relationship between $\frac{C_x}{C_o}$ to the coupling coefficient, k_t^2, wider bandwidth filters are more easily designed using resonators with higher k_t^2, and are more difficult to design with microresonators that have lower k_t^2. This limitation often leads designers to construct filters with more complicated topologies to achieve wider bandwidths. The maximum achievable fractional bandwidth of filters versus different topologies is also directly related to the k_t^2 of

the resonators used in the filter (18). Single-ended input and output topologies have difficulty in exceeding fractional bandwidths that are greater than 0.45 times the k_t^2 of the resonators, with ladder configurations reaching about 3% fractional bandwidths for resonators with 7.5% k_t^2 (18).

The key to being able to use temperature compensated AlN microresonators with bandwidths in the range of their ~1% k_t^2 is to negate the problematic effects of C_o when multiple resonators are cascaded in series. To study this, a two-pole synchronous filter circuit is used to investigate the effects of external passive reactive coupling components on the filter bandwidth, Figure 11 . The two separate resonators in this two-pole filter are identical, and they are each created by a parallel combination of 15 individual 4-finger electrode temperature compensated AlN microresonators. The parallel combination of 15 resonators effectively operates as a single microresonator with an optimized motional impedance (see previous section) with the equivalent circuit values in Table 1.

Table 1: Equivalent circuit values for a parallel configuration of 15, 4-finger electrode AlN microresonators

Variable	Value
$C_{ft1,2}$	75 fF
$C_{o1,2}$	5.062 pF
$R_{x1,2}$	7.4 Ω
$L_{x1,2}$	4768.017 nH
$C_{x1,2}$	0.022 pF

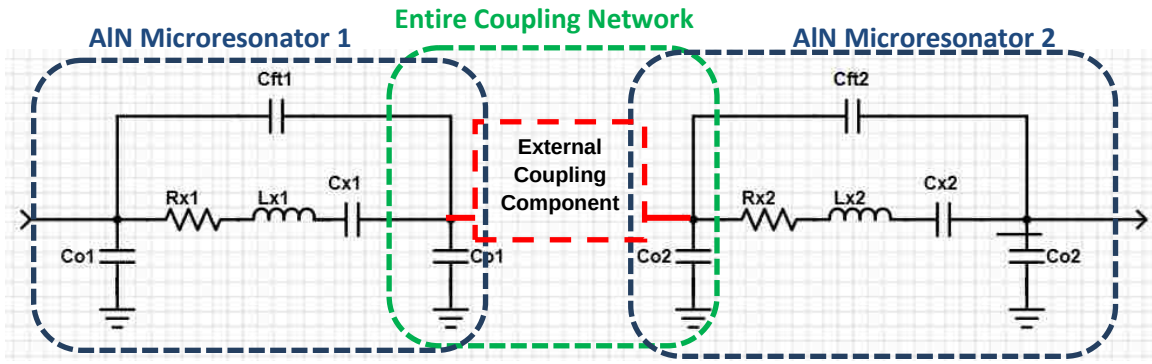

Figure 11: Two-resonator, synchronous filter equivalent circuit. AlN Microresonator 1 is exactly identical to AlN Microresonator 2 with the values in the table above.

From examination of the two-pole filter circuit, Figure 11, in order to counteract the bandwidth limiting effect of C_{o1} and C_{o2}, a shunt inductance in parallel with those capacitors could be inserted as an external coupling component to form a parallel LC tank circuit for the entire coupling network, Figure 12.

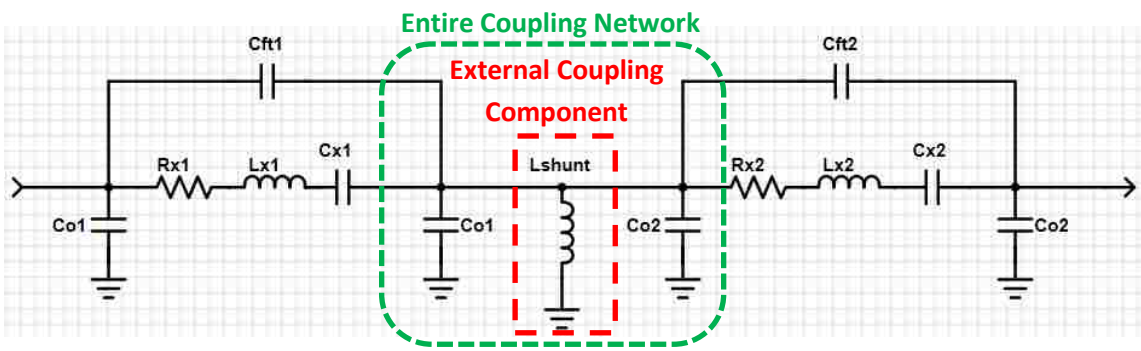

Figure 12: Two-pole, synchronous filter with external shunt inductor coupling.

Since C_{o1}=C_{o2}=5.062 pF, the inductance needed to resonate with the total shunt capacitance of the coupling network at the center frequency of the filter (500 MHz) would be 10nH from equation [15].

$$f = \frac{1}{2\pi\sqrt{LC}} \qquad [15]$$

The admittance of only the circuit labeled “Entire Coupling Network” in Figure 12, in isolation, without the rest of the filter’s circuit components, with the two C_o components, and L_{shunt} = 10 nH with Q=20 is shown in Figure 13(a). Figure 13(b) compares the effect on the filter bandwidth by introduction of this external shunt inductance. The filter response of the equivalent circuit of Figure 10, with only the coupling effect of the intrinsic C_{o1} and C_{o2}, is plotted in blue and red, along with the filter response of the circuit with the external shunt inductance coupling (purple and green) in Figure 13(b). Both equivalent filter circuits also had their termination impedances at their input and output ports changed from the nominal 50 Ω to 1 Ω to remove the Q-loading effect of the termination impedance on the resonators that would smooth out the poles and make the pole splitting less apparent.

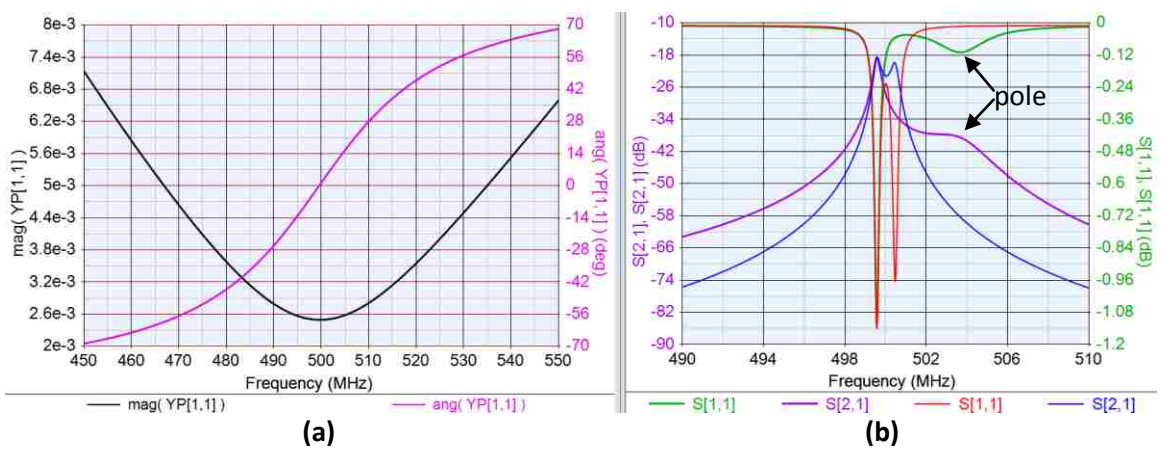

Figure 13: (a) Admittance magnitude and phase of just the coupling network of Figure 12 with Lshunt=10 nH, C_{o1}=C_{o2}=5.062 pF. (b) S-parameters of the entire filter circuit of Figure 12 with Lshunt=10 nH (green and purple), and the filter circuit of Figure 10 without Lshunt (blue and red), and the values in Table 1: Equivalent circuit values for a parallel configuration of 15, 4-finger electrode AlN microresonatorsTable 1.

With the introduction of this external shunt inductance, the admittance magnitude of the entire coupling network, without the other circuit components in the filter, reaches a minimum at 500 MHz as expected, indicating maximum impedance to ground at the node between the two resonators on resonance of the parallel LC tank circuit. This means that this shunt inductance has negated the effect of C_{o1} and C_{o2} at the filter's center frequency by resonating with the intrinsic shunt capacitances to form an effective open circuit. The phase of this admittance can also be seen to cross 0° at 500 MHz, indicating a point at resonance where the susceptance changes from inductive (or negative in polarity) to capacitive (positive in sign). This indicates that changes to the shunt inductance around this 10 nH value, could be used to adjust the coupling network's susceptance to be either capacitive or inductive.

The blue and red traces in Figure 13(b) are the transmission and reflection parameters for the original filter circuit of Figure 10, where the two poles of the filter, coupled only by the intrinsic C_{o1} and $C_{o2,}$ are readily apparent. With the insertion of an external coupling L_{shunt} into the filter circuit, the higher frequency pole of the original filter is pulled further away towards the higher frequency side of the filter. This indicates that the shunt inductance has reduced the coupling network's shunt capacitance due to the parallel combination of C_{o1} and C_{o2}, to a smaller capacitance that allows one of the poles of the filter to be tuned higher in frequency. As the shunt inductance is reduced below the 10 nH, the impedance of the coupling network becomes slightly inductive as shown in the Smith Chart of Figure 14(a).

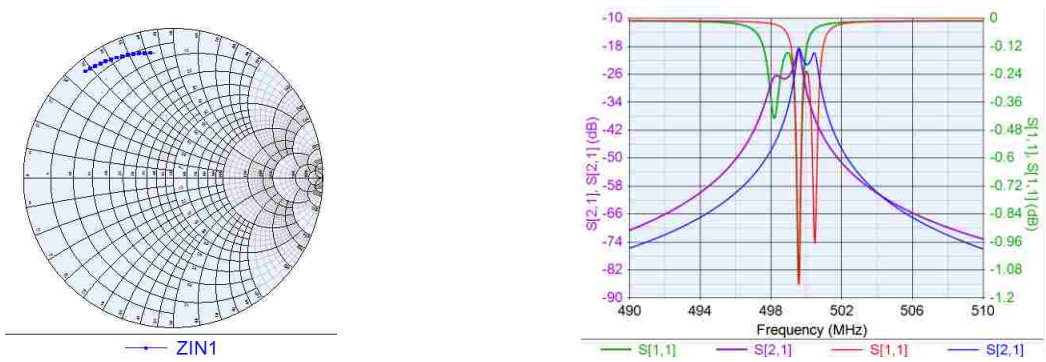

(a) **(b)**

Figure 14: (a) Impedance of just the coupling network of Figure 12 with Lshunt=5 nH, C_{o1}=C_{o2}=5.062 pF (b) S-parameters of the entire filter circuit of Figure 12 with Lshunt=5 nH (green and purple), and the filter circuit of Figure 10 without Lshunt (blue and red), and the values in Table 1: Equivalent circuit values for a parallel configuration of 15, 4-finger electrode AlN microresonatorsTable 1.

With this inductive admittance, the filter response, Figure 14(b), shows the filter poles now being tuned lower in frequency than the original center frequency of the filter's resonators. The external shunt inductance used in the coupling network can be used to create either an inductive or capacitive susceptance in combination with the intrinsic shunt capacitances of the resonators that are being coupled. When there is a capacitive susceptance, the poles of the filter can be tuned higher in frequency and with an inductive susceptance the poles are tuned lower in frequency.

Figure 15 similarly shows the coupling network's impedance and the filter response when the shunt capacitance is greater than 10 nH.

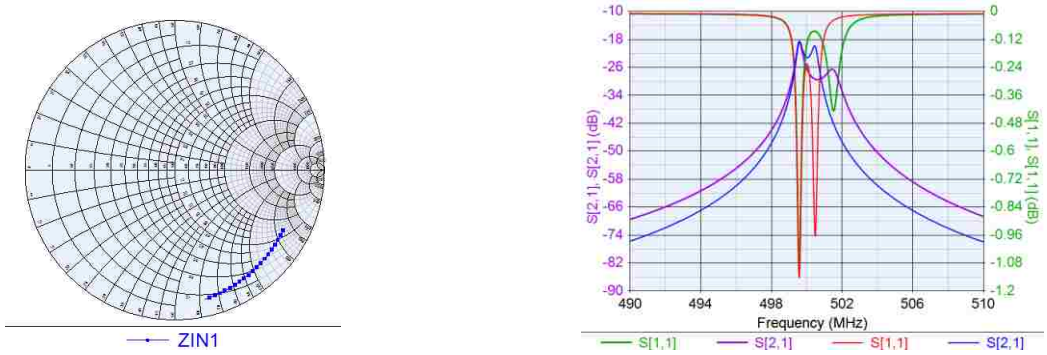

(a) (b)

Figure 15: (a) Impedance of the coupling network when Lshunt=15 nH (b) S-parameters of the entire filter circuit of Figure 12 with Lshunt=15 nH (green and purple), and the filter circuit of Figure 10 without Lshunt (blue and red), and the values in Table 1: Equivalent circuit values for a parallel configuration of 15, 4-finger electrode AlN microresonatorsTable 1.

The admittance becomes capacitive and filter response shows the second pole being tuned higher in frequency than the original center frequency of the filter allowing a wider bandwidth to be created by tuning the poles to a higher frequency.

Still problematic, however, is the low Q of the resonator shunt capacitances. For CMOS integration, on-silicon inductors with high Q are difficult to manufacture as well. The flexibility of using lower Q reactive components is a great benefit in the synthesis of wider bandwidth filters. As a filter's poles are tuned farther away in frequency from the original center frequency of the resonant circuits that form it, more energy needs to be stored in the coupling network components (16). The further away a pole is moved from the filter's original center frequency, the more attenuated the pole becomes and the more difficult it is to impedance match for a wide bandwidth filter. This problem makes it challenging to realize wider

bandwidth filters without the need for exceedingly high Q reactive components. The effect of low Q for the coupling components is demonstrated in Figure 16.

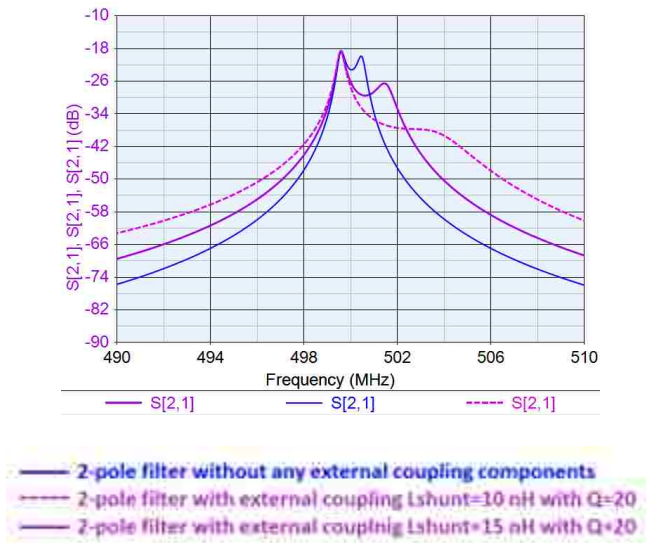

Figure 16: Effect of coupling network Q on filter transmission parameters. Q of C_{o1} and C_{o2} is 35, and Q of L_{shunt} is 20.

Figure 16 shows the higher frequency pole of this two pole filter in three different scenarios. For the blue trace, the filter's resonators are only being coupled by their respective $C_{o,}$ with the Q of C_{o1} and C_{o2} being 35. The two poles of the filter are only moved slightly away from the resonators' initial center frequency of 500 MHz and the amplitudes of the poles are fairly even and at ~-20 dB. When an external shunt inductance of 10nH with a Q of 20 is used to couple the resonators, the filter's higher frequency pole is moved approximately 3.5 MHz away from the resonators' original center frequency of 500 MHz and its amplitude is attenuated to -38 dB. As this coupling shunt inductance is increased to 15 nH, with the same Q=20, this higher frequency pole moves closer to the filter's original 500 MHz center frequency and the amplitude of the pole becomes less

attenuated, -26 dB. The attenuation of the tuned pole can easily been seen to worsen as the pole is moved further away from the filter's original center frequency. The more a pole is attenuated, the more difficult it becomes to impedance match the filter to create a wide 3 dB bandwidth because the loss in the two poles of the filter are so different. Figure 17 shows the same filter response if the same coupling shunt inductance of L_{shunt} = 10 nH has a Q of 200 instead of 20. The new pole is sharper and less attenuated if L_{shunt} has a 10x higher Q but is still limited by the low Q of the resonator shunt capacitance.

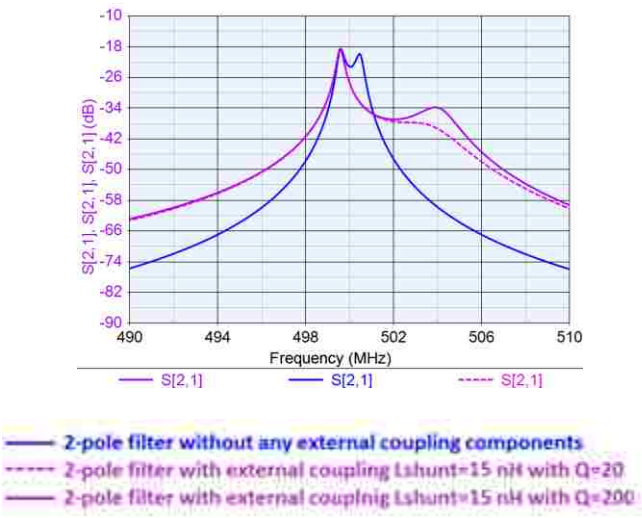

Figure 17: Effect of Q on filter poles

A shunt inductor coupling has thus been shown to resonate with the problematic shunt capacitance with the capability of tuning the filter poles either higher in frequency or lower, depending on whether the coupling network's admittance is capacitive or inductive. Inclusion of a series inductance into the coupling network can be used to tune the poles of a filter in the opposite direction. Using these coupling components together in a network, the poles of the filter could be tuned

in both the higher and lower frequency directions so that a wider bandwidth could be achieved by moving each pole half the desired bandwidth's distance. This would minimize the detrimental effect of low Q components for filter synthesis methods where one pole is tuned over the majority of the frequency distance to obtain the desired bandwidth. This also allows the loss in both of the poles to be identical, making matching of the filter much less problematic.

A pi-network of inductors was considered to create a filter bandwidth wider than the limit set by the 1% k_t^2 of the microresonators with the equivalent circuit of Figure 18.

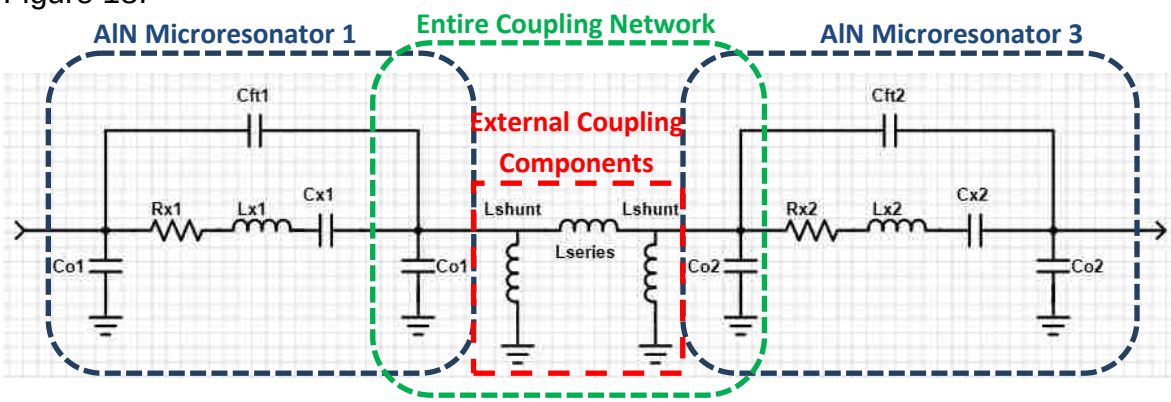

Figure 18: Two-pole synchronous filter with external inductor pi-network coupling.

Two external shunt inductors could be used to resonate with the C_o of each resonator that was being coupled, and the inductance could be used to tune the poles either higher or lower in frequency. The series coupling inductance, L_{series}, could be used to tune the poles in the opposite direction in frequency.

First, the effect on the filter poles using only a series coupling inductor is studied. When an external coupling series inductor is used to create the filter circuit of Figure 19, for L_{series} = 20 nH, looking from the input, the series inductor resonates

with C_{o2} to create a maximum admittance, or minimum impedance to ground at the node between the resonators at 500 MHz.

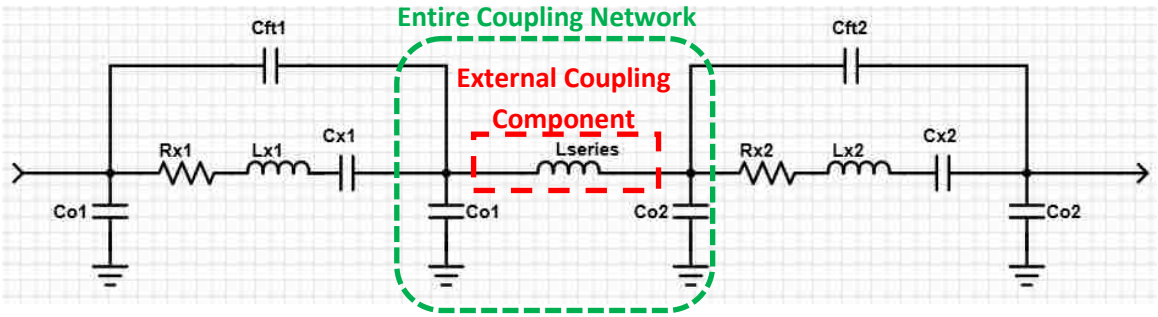

Figure 19: Two-pole synchronous filter with an external series inductor coupling.

The admittance of this coupling network when L_{series} = 20 nH also transitions between capacitive below 500 MHz to inductive above 500 MHz, Figure 20(a). The filter response Figure 20(b) shows one of the filter poles being tuned lower in frequency with this series inductance. This lower frequency pole is tuned by adjusting L_{series} around 20 nH to present either inductive or capacitive admittances that adjust the distance that this lower frequency pole moves away from the original filter's center frequency. Around 20 nH, if the admittance is capacitive, the lower frequency pole moves lower in frequency, and when the admittance is inductive, the lower frequency pole moves closer to the center frequency.

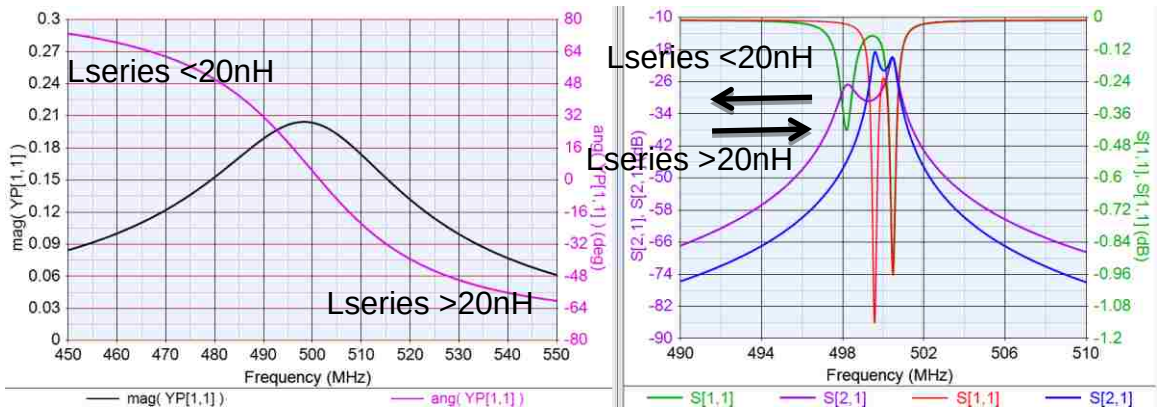

(a) **(b)**

Figure 20: (a) Admittance magnitude and phase of only the coupling network of Figure 19 with Lseries=20 nH, C_{o1}=C_{o2}=5.062 pF (b) S-parameters of the entire filter circuit of Figure 19 with Lseries=20 nH (green and purple), and the filter circuit of Figure 10 without Lseries (blue and red), and the values in Table 1: Equivalent circuit values for a parallel configuration of 15, 4-finger electrode AlN microresonatorsTable 1.

However, for the series inductor coupling, there is a second resonance when L_{series} resonates with the series combination of C_{o1} and C_{o2} since the capacitances share a ground node. This resonance between L_{series} with C_{o1} + C_{o2} occurs when L_{series} = 40 nH. When the series inductance is 40 nH, Figure 21, the admittance of the coupling network formed by C_{o1}, C_{o2}, and L_{series} behaves very similarly to the shunt inductor coupling network that resonated out the shunt capacitances in Figure 13. This larger series inductance tunes the higher frequency pole, with higher series inductance values tuning the higher frequency pole closer to the filter's original center frequency.

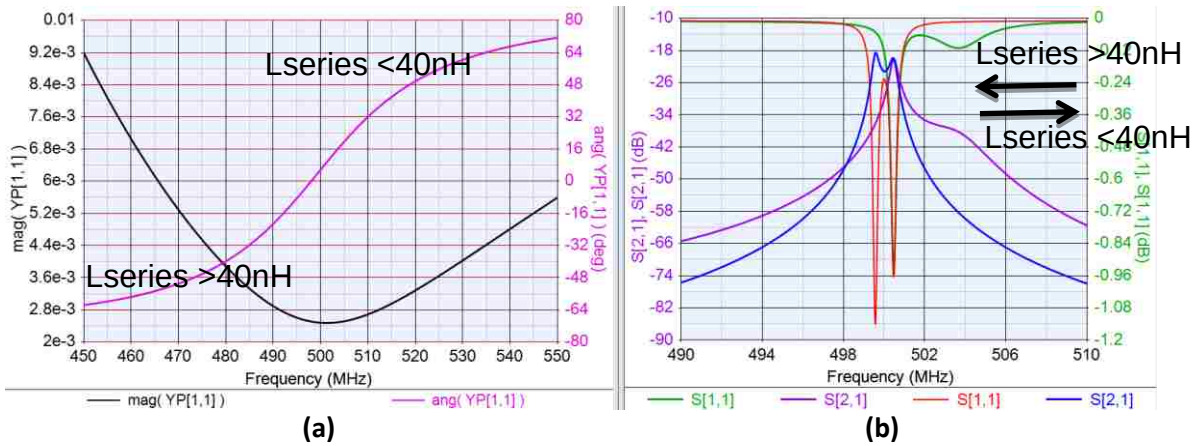

Figure 21: (a) Admittance magnitude and phase of only the coupling network of Figure 19 with Lseries=40 nH, C_{o1}=C_{o2}=5.062 pF. (b) S-parameters of the entire filter circuit of Figure 19 with Lseries=40 nH (green and purple), and the filter circuit of Figure 10 without Lseries (blue and red), and the values in Table 1: Equivalent circuit values for a parallel configuration of 15, 4-finger electrode AlN microresonatorsTable 1.

Combining the effects of the shunt and series inductor into an inductor pi-network would allow independent tuning of both poles of the resonators that are being coupled. The shunt inductances of the pi-network would each need to resonate with the shunt capacitance adjacent to them, Figure 22. The shunt inductances would then have to be 20 nH each.

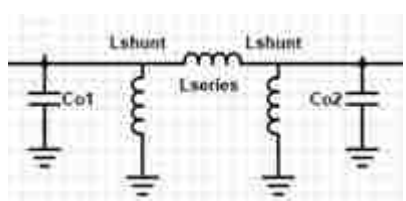

Figure 22: Filter coupling network with an inductor pi-network schematic.

Once the shunt inductances were selected to resonate with the resonators' C_o, a small, 1 nH series inductance is inserted in between the shunt inductors. Figure 23 shows the admittance of Figure 22's coupling network with L_{shunt}=20 nH and L_{series}=1 nH. This is the familiar response where the phase of the network hovers

between inductive and capacitive with minimal admittance at the filter's 500 MHz center frequency.

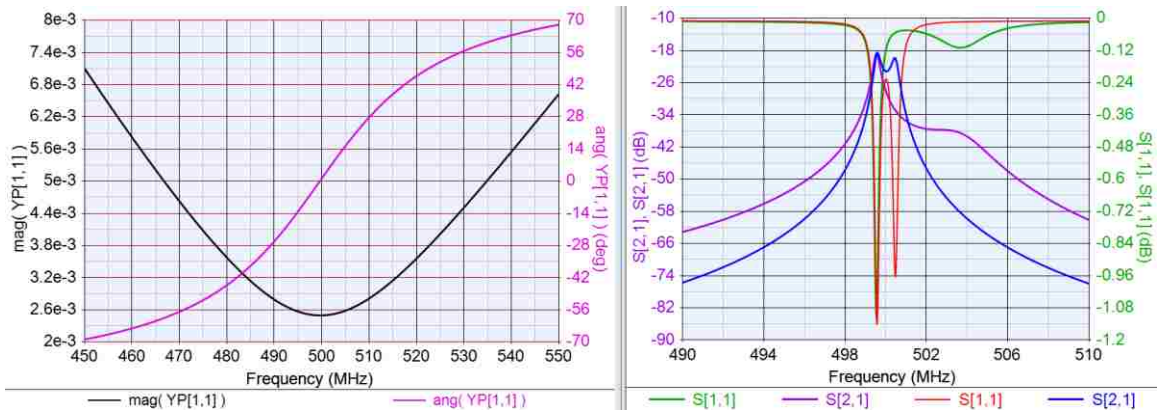

(a) **(b)**

Figure 23: (a) Admittance magnitude and phase of the coupling network of Figure 22 with Lshunt=20 nH, Lseries=1 nH, C_{o1}=C_{o2}=5.062 pF. (b) S-parameters of the entire filter circuit of Figure 18 with Lshunt=20 nH, Lseries=1 nH (green and purple), and the filter circuit of Figure 10 without an external coupling components (blue and red), and the values in Table 1: Equivalent circuit values for a parallel configuration of 15, 4-finger electrode AlN microresonatorsTable 1.

At this point, it was easily observed that increasing the series inductance of the pi-network served to tune the higher frequency pole of the filter closer towards 500 MHz, while increasing the shunt inductances tuned the lower frequency pole further below 500 MHz. The poles were thus tuned to each be 2.5 MHz away from the center frequency with L_{shunt}=26nH and L_{series}=33nH, all with Q=20, Figure 24.

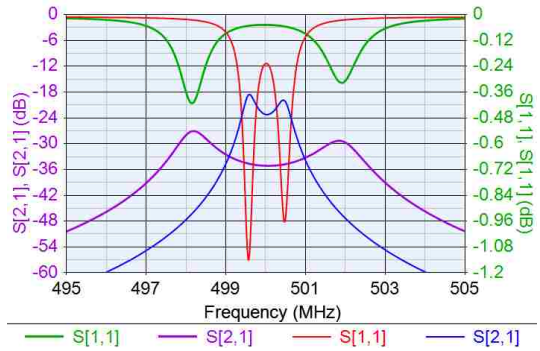

Figure 24: S-parameters of the entire filter circuit of Figure 18 with Lshunt=26 nH, Lseries=33 nH (green and purple), and the filter circuit of Figure 10 without an external coupling components (blue and red), and the values in Table 1: Equivalent circuit values for a parallel configuration of 15, 4-finger electrode AlN microresonatorsTable 1.

Because each pole was tuned to be just half the desired bandwidth away in frequency from the filter's initial center frequency, the low Q of the components in this coupling network are able to store and transfer the energy between the resonators without significantly attenuating the tuned poles. More importantly, the loss of the two poles of the filter are identical, making matching of the filter possible. A greater than 1% relative bandwidth filter can therefore be realized using temperature compensated AlN microresonators with k_t^2 = 1%, despite the presence of the C_o elements, using low Q inductors that could be manufactured on silicon. These inductances needed for the coupling network are also available as standard value, low Q COTS inductors.

These findings were extrapolated to a three-pole, synchronous filter design, Figure 25. The third resonator stage was needed to improve the shape factor for the filter from the two-pole design. The three-pole design similarly required the series coupling inductances to be 33nH, and the shunt coupling inductance

values were 26nH for an over-designed relative bandwidth of 1.06% or 5.3MHz bandwidth at 500MHz center frequency, Figure 26.

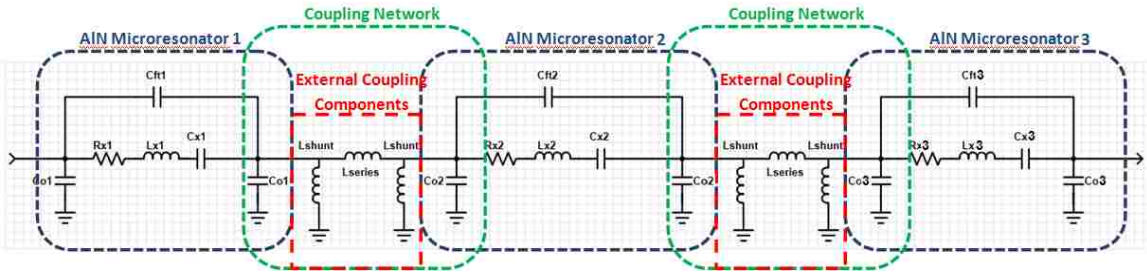

Figure 25: Equivalent circuit for three-pole synchronous filter with external inductor pi-network coupling

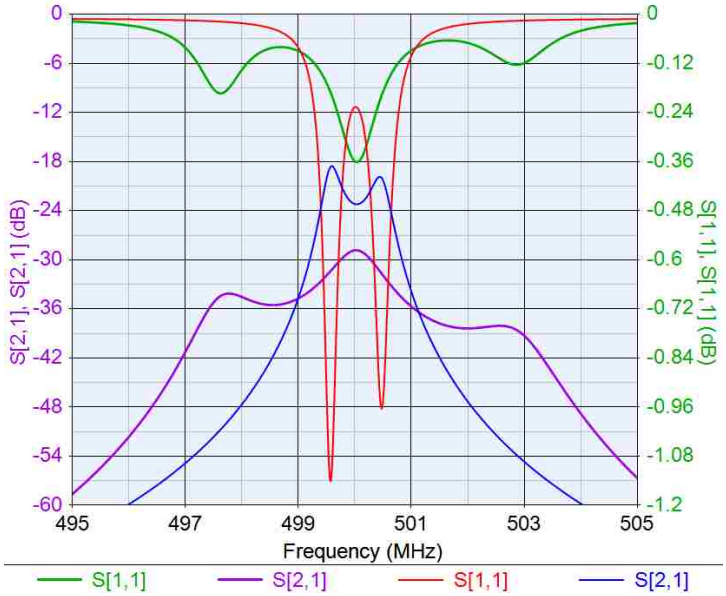

Figure 26: Transmission and reflection parameters of the entire three pole filter circuit Figure 25 when Lshunt=26nH and Lseries=33nH, overlaid on same parameters for the two-pole filter with no external coupling components.

Matching Network

Matching networks using reactive components are needed to match the input and output impedance of the filter to the 50Ω characteristic impedance of the system that would utilize this IF filter. To create a maximally flat, or Butterworth,

(20) filter transfer function over the band-pass frequency range, and to improve the ripple of the band-pass group delay, impedance matching networks were also designed. An L-network, Figure 30, with increasing shunt capacitance and an increasing series inductance was needed to impedance match this filter, as found using Smith Chart graphical impedance matching solutions technique (20). This was also performed using Genesys simulation software.

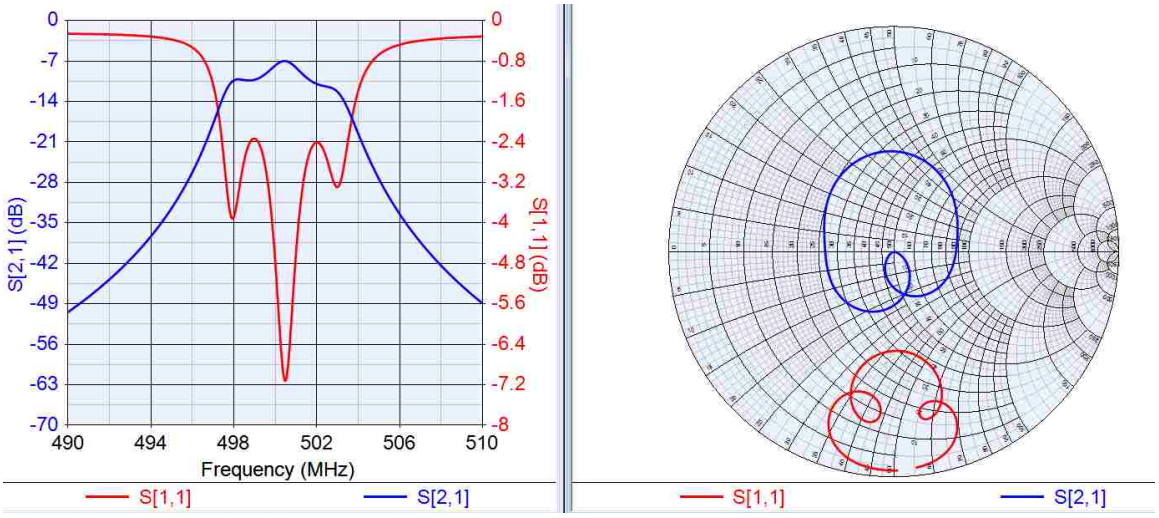

Figure 27: Unmatched 3-pole filter simulated S-parameters in log-magnitude form and on a Smith Chart .

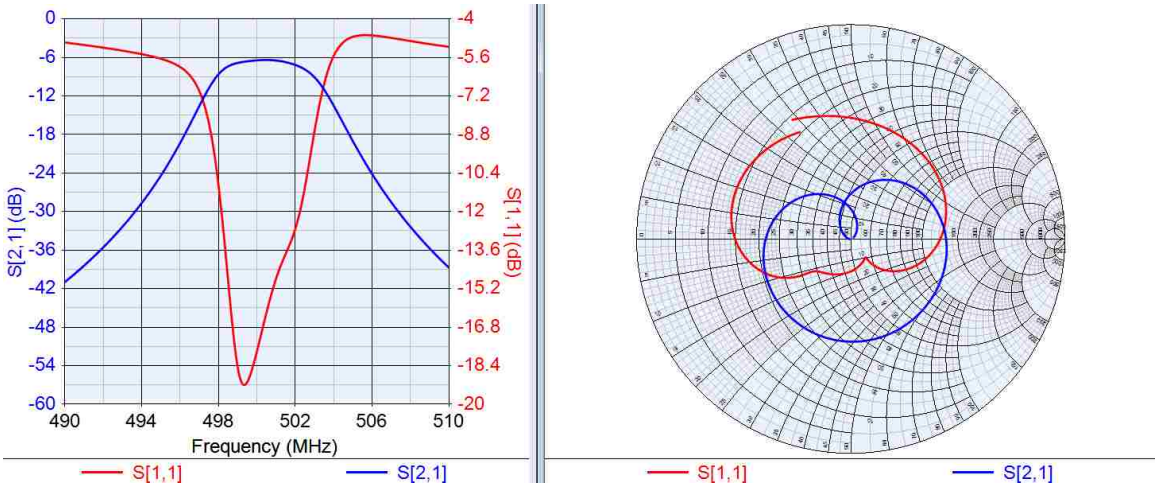

Figure 28: Impedance matched 3-pole filter simulated S-parameters parameters in log-magnitude form and on a Smith Chart. Bandwidth=5.3MHz at a center frequency of 500.475MHz.

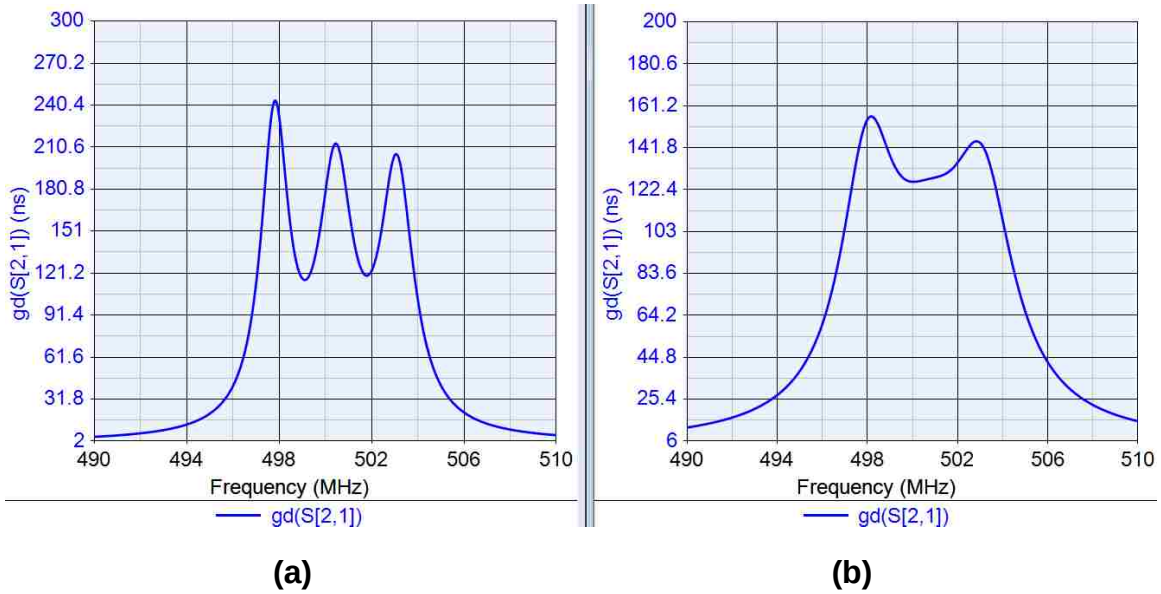

Figure 29: (a) Unmatched, 500 MHz filter's simulated group delay (b) Same parameters for the filter once matched to 50Ω termination impedance.

Figure 30 is the complete circuit design schematic with the coupling and matching networks.

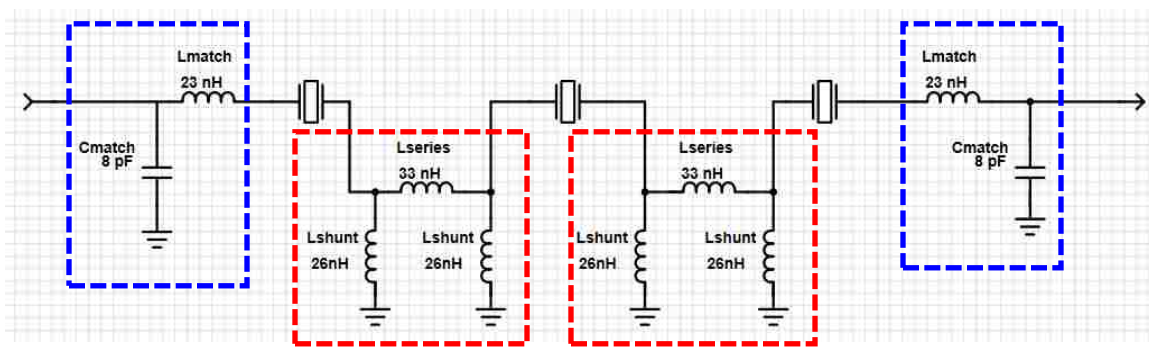

Figure 30: Complete 500MHz filter design with 5MHz bandwidth equivalent circuit with coupling networks (red boxes) and matching networks (blue boxes). The crystal resonator components each represent 15 temperature compensated AlN microresonator circuits in parallel.

The crystal resonator components are all at the same center frequency of 499.82 MHz and each crystal resonator encapsulates the parallel circuit combination of fifteen identical, four-finger electrode temperature compensated AlN

microresonators that function as effectively one resonant circuit with an Rx=7.4Ω for the AlN microresonator circuits, as drawn in Figure 25.

Filter Layout

Initially, this filter is going to be implemented on a PCB with off-chip coupling and matching components. Planar inductors fabricated on a silicon substrate are in the process of being fabricated, Figure 31, and then the potential to integrate the coupling and matching components with this filter can be demonstrated. The components needed for the coupling and matching networks are standard value inductors and capacitors with low Q that are readily available as COTS for the PCB implementation.

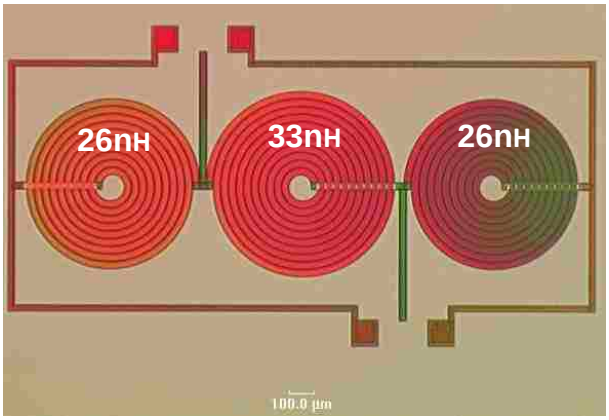

Figure 31: Microscope picture of partially fabricated inductor pi-network to be used for on-chip integration with filter.

This filter design required an R_x=3.7Ω, while the fundamental resonator design was measured to have a motional impedance of 56Ω. To create a resonator with the proper motional impedance, fifteen of the 56Ω four-finger-electrode

resonators were laid out in parallel, effectively creating a single resonator with the same center frequency but with much lower motional impedance.

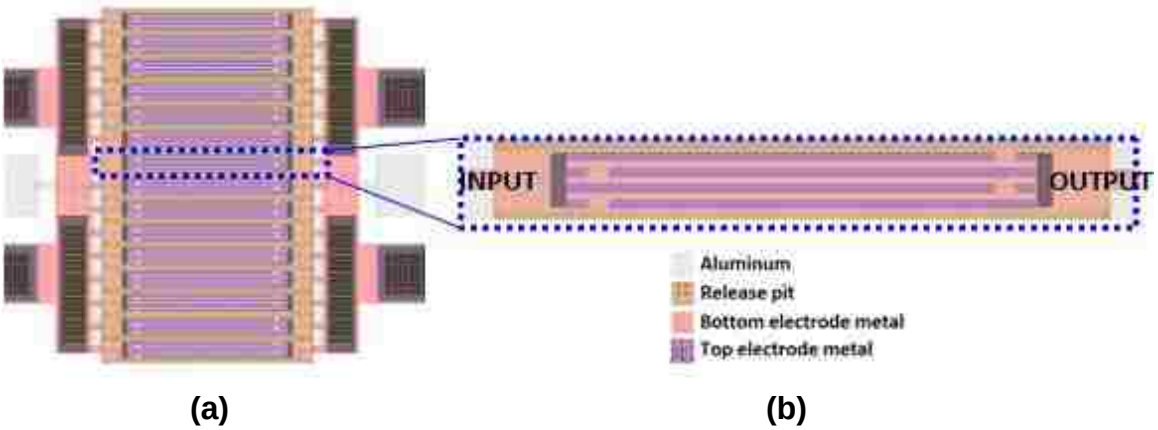

Figure 32: (a) Layout of one of the three AlN microresonator's needed for the filter. This resonator is made up of 15 identical four-finger electrode individual microresonators connected in parallel. (b) Layout of one of the four-finger electrode AlN microresonators.

The width of the resonator, the vertical dimension in Figure 33, sets the frequency of the resonator, as it is the direction of propagation for the microresonator's standing wave.

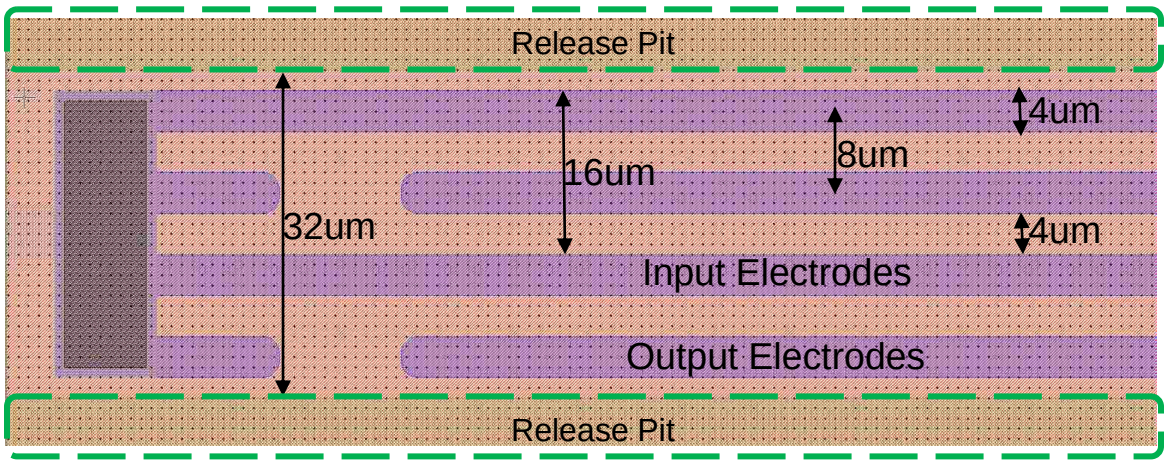

Figure 33: Close-up of one side of a four-finger electrode temperature compensated AlN microresonator.

This width is defined lithographically, by drawing a “release pit”, which is vertically etched through the aluminum nitride, bottom metal layers, and temperature compensating oxide. The release pit etch also exposes the poly-silicon release layer that is underneath the entire resonator body from the top. Exposing the poly-silicon allows XeF_2 to access and etch away the poly-silicon under the resonator at the end of the fabrication processing in order to suspend the resonator. This suspension provides mechanical isolation in air on all sides, keeping the mechanical wave trapped in the thin-film membrane, without mechanical losses other than at the tether points on the INPUT and OUTPUT sides or through air damping.

The electrodes are made of the “top electrode metal” layer, which is actually two layers of 100nm of aluminum copper (Al-Cu) and 25nm of titanium nitride (TiN). Since the resonator center frequency needed for this filter was determined to be 499.82MHz, using the velocity of 7998 m/sec extracted from the single, four-finger electrode temperature compensated AlN microresonator measurement, the wavelength, λ, is 16um. The width of the electrodes was then drawn to be $\lambda/4$ = 4um, and with the pitch between the inter-digitated input and output electrodes equal to $\lambda/2$ = 8um, this leads to a spacing between electrodes of $\lambda/4$. With this four-finger electrode resonator design, this required the total resonator width to be 32um.

An aluminum layer is used as the interconnect metal to route the parallel combination of 15 resonators, and to function as the electrical contact to resonator input and output electrodes. The bottom metal layer is the electrical

ground plane for the resonator and vias are drawn to give contact to the bottom metal layer from the top surface of the substrate. Contact pads to the input and output ports of the resonators for RF probe station testing and wirebonding were laid out as standard, 100um x 100um square, ground-signal-ground pads with a 150 µm pitch. This filter design requires three, identical resonant circuits, each with a center frequency of 499.82 MHz and an R_x=3.7Ω, so this identical resonator was laid out three times on a single die which could later be singulated for integration onto a PCB.

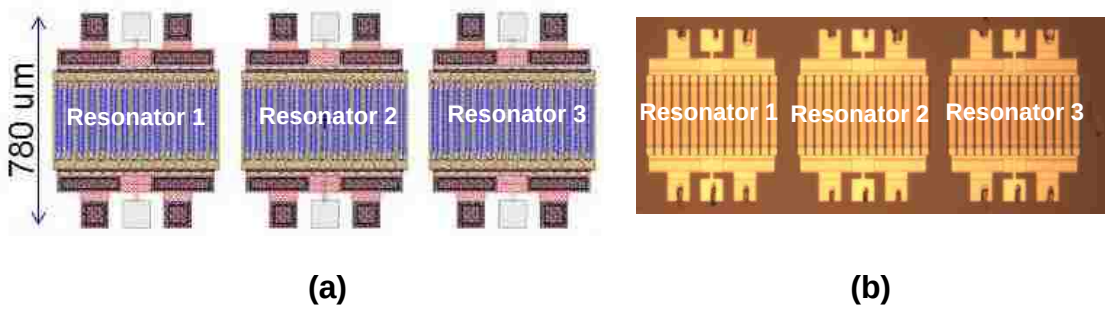

Figure 34: (a) Layout of the three, temperature compensated AlN microresonators for the filter design (b) Fabricated resonators.

CHAPTER 4

Measurements

Once the temperature compensated AlN microresonators had been fabricated at Sandia National Laboratories' MESA facility, the resonators' S-parameters were tested using an Agilent E5071C network analyzer. Though the resonators were designed and laid out to be identical, non-uniformities inherent to microfabrication process are known to cause variations in device parameters such as center frequency. Because the synchronous filter designs have better insertion loss, requiring three resonators with identical center frequencies, a single die was selected where all three resonators had very close to identical center frequencies. The measurements for the three resonators on this single die are shown in Figure 35. The center frequency for one of the resonators, the blue data trace, can be seen to be slightly different than the other two resonators on that die. Also, the center frequency of the resonators turned out to be slightly lower than the designed values which can be trimmed later via annealing (21).

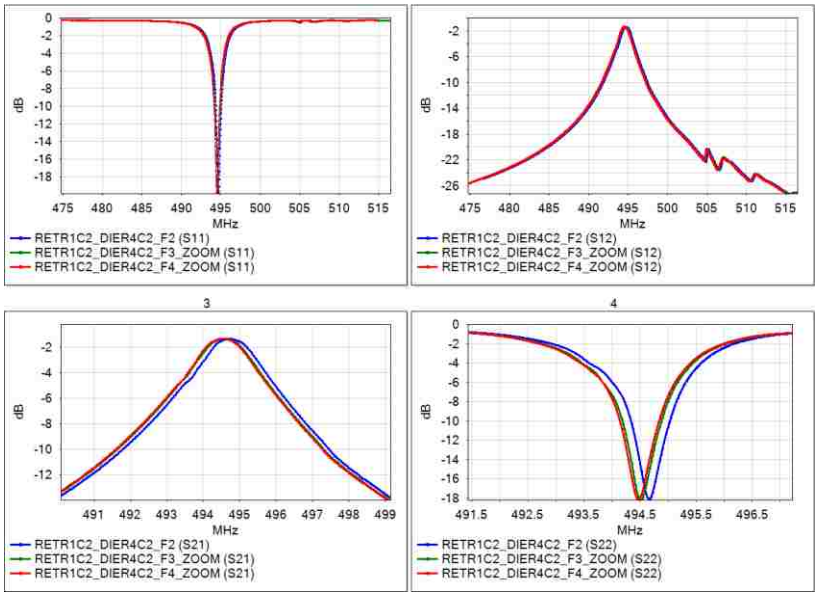

Figure 35: S-parameters for three, temperature compensated AlN microosresonators on a single die.

These S-parameter measurements were then imported into Genesys simulation software, Figure 36, and integrated with the inductor pi-network coupling and matching networks.

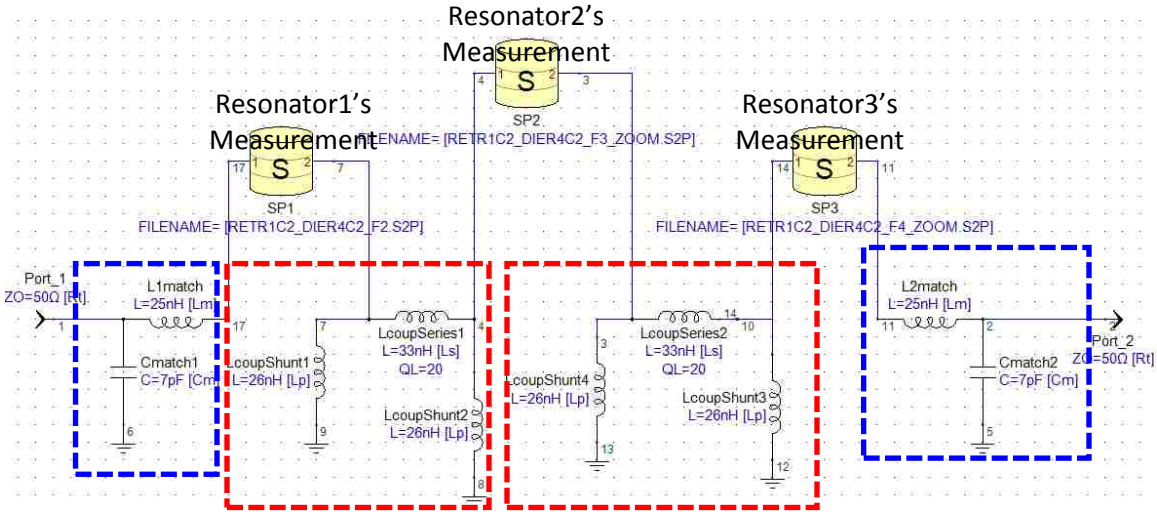

Figure 36: Genesys simulator integrating resonator measurements with coupling networks (red boxes) and matching networks (blue boxes).

Figure 37 is the simulated filter response using the real resonator measurements with the original predicted inductor coupling values.

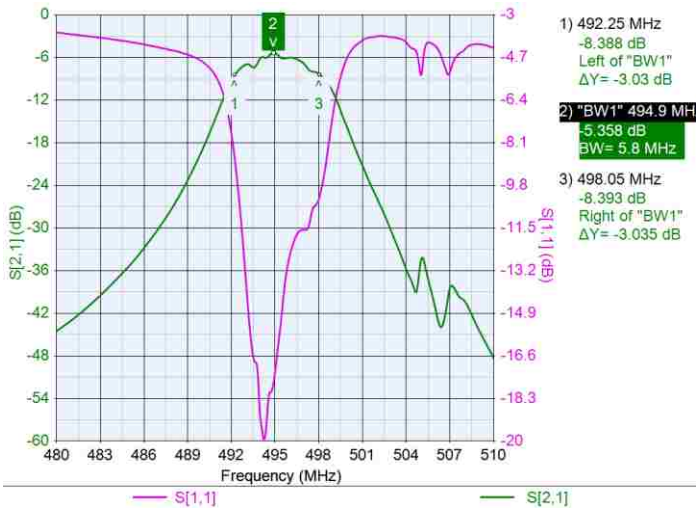

Figure 37: Simulation data using real resonator measurements with the inductor and capacitor coupling and matching components integrated.

To get the flattest pass-band response using the actual measured resonators, the matching network needed to be changed by 1nH and 1pF from the predicted values. Because the center frequency of the resonators turned out to be slightly lower than the targeted frequency of 500 MHz, the original filter design circuit was shifted only in frequency to compare the predicted filter response versus the data with the real measurements, Figure 38. All of the other original designed values for the resonators and the coupling and matching network values were maintained. The filter response using the measured data turned out to have a 5.8 MHz bandwidth with a center frequency of 494.9 MHz with an insertion loss of -5.358 dB.

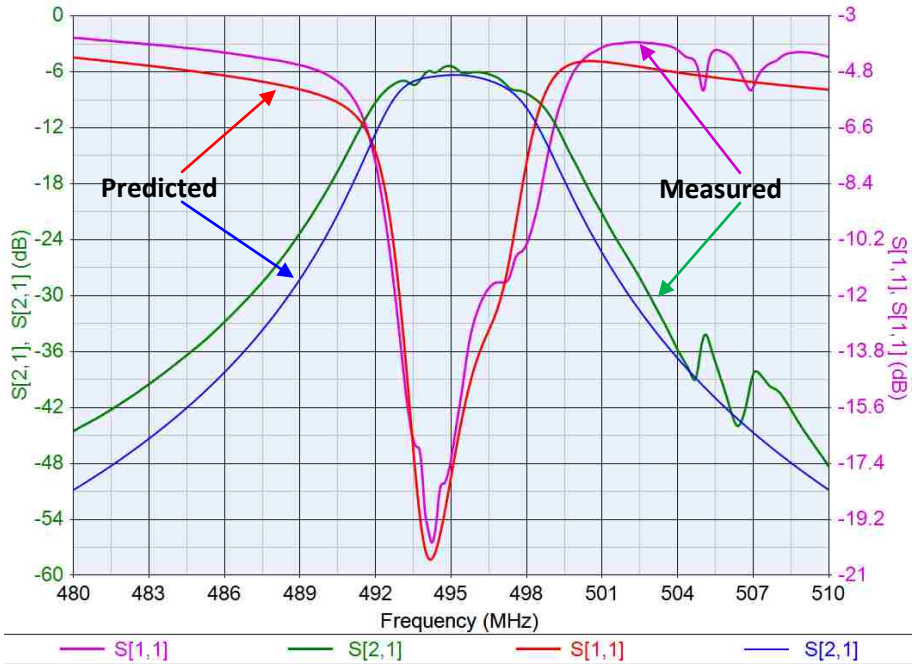

Figure 38: S-parameters comparing the measured data with the original filter design downshifted in frequency only. The original designed coupling and matching network components were maintained.

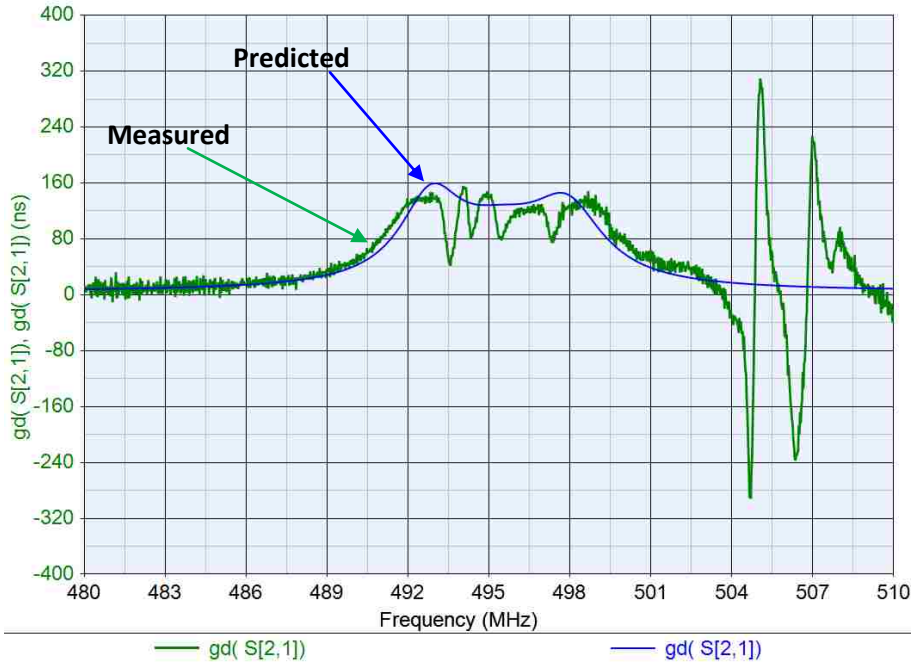

(a) **(b)**

Figure 39: Group delay for the filter response using measured data versus the original filter design downshifted in frequency only. The original designed coupling and matching network components were maintained.

There is some slight ripple in the pass-band, < 0.5 dB, likely due to weak spurious modes in the resonator that combine and amplify with the three resonator stages in this filter. A filter using these actual devices, as simulated with the coupling inductors, should be able to be realized with series coupling inductances of 33nH and shunt inductances of 26nH as originally predicted. The matching networks require 25nH series inductors and 7pF shunt capacitors at the filter input and output. All of these passive reactive components are standard values readily available off the shelf, especially since they need only be low Q (a Q of 20 was used for all of the external reactive components).

Finally, to characterize the temperature compensation of these resonators, S-parameters for an identically designed resonator from a separate die from the same wafer was measured at 100C, 80C, 60C, 40C, and 25C. Using Equation [16], the temperature coefficient of frequency (TCF), for these resonators is +2.75 ppm/C.

$$\text{TCF in ppm} = \frac{(f_{temperature1} - f_{temperature2}) * 10^6}{(temperature1 - temperature2) * faverage} \qquad [16]$$

$$\Delta_{\text{frequency}} = \frac{center\ frequency * ppm}{10^6} \qquad [17]$$

Temperature (°C)	Center Frequency (MHz)	Insertion Loss (dB)
100	485.800000	-1.13
80	485.781250	-1.15
60	485.762500	-1.13
40	485.718750	-1.18
25	485.700000	-1.25

Table 2: Resonator temperature Coefficient of Frequency measurements

This indicates the filter will drift in center frequency by 240 kHz over a temperature range from -55 to 125 C, or less than 0.05% of the 5.8 MHz filter bandwidth. The insertion loss is also seen to be extremely stable across temperature as well, with a maximum variation of just 0.12 dB over the temperature range.

CHAPTER 5

Conclusions

A very temperature stable, 1.17% relative bandwidth filter near the designed 500 MHz center frequency was successfully implemented as verified by measurements of fabricated AlN microresonators coupled by an inductor pi-network of low Q (Q=20) inductors. The frequency error is due to thin film variation and recently developed techniques (21) can be used to permanently shift the center frequency of the resonators slightly upwards to reach the proper value. Though the entire filter has not been fully, physically realized, pending a full integration of the resonator MEMS die with off-chip inductors on a PCB, the agreement between the initial simulated design using the temperature compensated AlN microresonator equivalent circuit model and the simulation of the inductor network with actual resonator measurements is promising. The study of low-Q, passive reactive components to couple AlN microresonators indicates that bandwidths ranging from extremely narrow, as limited by the Q of the resonators, to fairly wide (~1.5%), can be realized depending on the coupling network topology. Of critical importance was the development of the inductor pi-network that was required to meet the filter fractional bandwidth requirements (1%) using low-Q coupling elements. This dramatically extended the maximum filter fractional bandwidth which was previously limited by the presence and low Q values of the resonator shunt capacitances. Attempts to reach the required filter bandwidth using only series or only shunt inductances failed because too

much energy was stored in the low Q coupling network for the widest pole splitting. The inductor pi-network allowed the two poles to be equally split around the natural resonance frequencies of the microresonators, enabling a doubling of the maximum filter bandwidth that can be achieve with low Q coupling elements. This capability along with the ability to manufacture resonators at completely different frequencies in a small space, side-by-side on a single die demonstrates the power AlN microresonators have as an attractive technology for RF communications. Temperature compensation and CMOS compatibility further enhance the benefits of AlN microresonators by offering higher selectivity and sensitivity while further miniaturizing the technology's physical footprint with single-chip integration.

Future work includes on-silicon inductor testing and development, awaiting the completion of an inductor study fabrication run. The next steps of this project include utilizing a newly developed technique (21) using rapid thermal annealing (RTA), to permanently shift the center frequency of these resonators slightly upwards to meet the specified 500MHz. A PCB also needs to be laid out with COTS coupling and matching components along with the MEMS die of the three resonators, which will be interconnected to the circuit with wirebonds. The entire physical filter will then be tested to characterize filter specifications, including measuring the entire PCB circuit over temperature to again verify TCF.

WORKS CITED

1. **Razavi, Behzad.** *RF Microelectronics.* s.l. : Prentice Hall, 1997.

2. *Direct-Conversion Radio Transceivers for Digital Communications.* **Asad A. Abidi, Senior Member, IEEE.** NO. 12, s.l. : IEEE JOURNAL OF SOLID-STATE CIRCUITS, DECEMBER 1995, Vol. VOL. 30 .

3. *Design of dissipative band-pass filters producing desired exact amplitude-frequency characteristics.* **Dishal, Milton.** s.l. : Proceedings of the IRE 37, 1949. no. 9 (1949): 1050-1069.

4. *Multi-Frequency Aluminum Nitride Micro-Filters for Advanced RF Communications.* **R. H. Olsson, K. E. Wojciechowski, M. R. Tuck, and J. E. Stevens.** s.l. : Goverment Microcircuit Application and Critical Technology Conference, 2010. pp. 257-260..

5. *COUPLING COEFFICIENTS OF RESONATORS IN MICROWAVE FILTER THEORY.* **Tyurnev, V.V.** s.l. : Progress In Electromagnetics Research B, 2010, Vols. 21, 47-67.

6. **Gianluca Piazza, Valeriy Felmetsger, Paul Muralt, Roy H. Olsson III, and Richard Ruby.** Piezoelectric aluminum nitride thin films for microelectromechanical systems. *Materials Research Society Bulletin.* 2012, Vol. 37, November.

7. **Piazza, Gianluca.** *Piezoelectric Aluminum Nitride Vibrating RF MEMS for Radio Front-End Technology.* BERKELEY : GRADUATE DIVISION OF THE UNIVERSITY OF CALIFORNIA, BERKELEY, 2001.

8. *Theory and Analysis of MEMS Resonators.* **Kaajakari, Ville.** s.l. : IEEE International Frequency Control Symposium, 2011.

9. *Single-chip precision oscillators based on multi-frequency, high-Q aluminum nitride MEMS resonators.* **Wojciechowski, K.E., Olsson, R.H., Tuck, M.R., Roherty-Osmun, E.** International : Solid-State Sensors, Actuators and Microsystems Conference, 2009. TRANSDUCERS IEEE.

10. **Pourkamali, Siavash.** *High Frequency Capacitive Single Crystal Silicon Resonators and Coupled Resonator Systems.* s.l. : Georgia Institute of Technology, 2006.

11. **Hashimoto, Ken-ya.** *RF Bulk Acoustic Wave Filters for Communications.* Norwood, MA 02062 : ARTECH HOUSE, 2009.

12. *VHF and UHF Mechanically Coupled Aluminum Nitride MEMS Filters.* **Roy H. Olsson III, Cody M. Washburn, James E. Stevens, Melanie R. Tuck and Christopher D. Nordquist.** s.l. : Frequency Control Symposium, 2008 IEEE International, pp. 634-639. IEEE, 2008.

13. *Post-CMOS-Compatible Aluminum Nitride.* **R. H. Olsson, K. E. Wojciechowski, M. S. Baker, M. R. Tuck, and J. G. Fleming.** no. 3, pp. 671–678, s.l. : Journal of Microelectromechanical Systems, 2009, Vol. vol. 18.

14. *Post-CMOS Compatible Aluminum Nitride MEMS Filters and Resonant Sensors.* **R. H. Olsson III, J. G. Fleming, K. E. Wojciechowski, M. S. Baker, and M. R. Tuck.** s.l. : IEEE International Frequency Control Symposium, pp. 412–419., 2007.

15. Rocking Curves & High Resolution Diffraction. *H&M Analytical Services.* [Online] [Cited: 6 16, 2013.] http://www.h-and-m-analytical.com/rocking_curves.shtml.

16. **III, Roy Olsson.** Microresonator Tutorial: Electrical Modeling. 2011.

17. **Zverev, Anatol I.** *Handbook of Filter Synthesis.* s.l. : John Wiley & Sons, 1967.

18. **Songbin Gong, Associate Member, IEEE, and Gianluca Piazza, Member, IEEE.** Design and Analysis of Lithium–Niobate-Based High Electromechanical Coupling RF-MEMS Resonators for Wideband Filtering. *IEEE TRANSACTIONS ON MICROWAVE THEORY AND TECHNIQUES.* 2013, Vol. 61, 1.

19. *Very High Frequency Channel-Select MEMS Filters Based on Self-Coupled Piezoelectric AlN Contour-Mode Resonators.* **Zuo, Cengjie.** 1-2, s.l. : Sensors and Actuators, May 2010, Vol. 160.

20. **Pozar, David M.** *Microwave Engineering.* s.l. : John Wiley & Sons, Inc., 2005.

21. **M. David Henry, Janet Nguyen, Travis Young, Todd Bauer and Roy H. Olsson III.** *Frequency Trimming of Aluminum Nitride Microresonators Using Rapid Thermal Annealing.* Albuquerque : Sandia National Labs, MESA Fabrication Facility, 2013.

Sandia National Laboratories is a multi-program laboratory managed and operated by Sandia Corporation, a wholly owned subsidiary of Lockheed Martin Corporation, for the U.S. Department of Energy's National Nuclear Security Administration under contract DE-AC04-94AL85000.